Molecular Therapy
Original Article

Loss of Shp2 Rescues BDNF/TrkB Signaling and Contributes to Improved Retinal Ganglion Cell Neuroprotection

Nitin Chitranshi,[1] Yogita Dheer,[1] Mehdi Mirzaei,[1,2,3] Yunqi Wu,[1] Ghasem H. Salekdeh,[2] Mojdeh Abbasi,[1] Veer Gupta,[4] Roshana Vander Wall,[1] Yuyi You,[5] Stuart L. Graham,[1,5] and Vivek Gupta[1]

[1]Faculty of Medicine and Health Sciences, Macquarie University, F10A, 2 Technology Place, North Ryde, NSW 2109, Australia; [2]Department of Molecular Sciences, Macquarie University, Sydney, NSW, Australia; [3]Australian Proteome Analysis Facility, Macquarie University, Sydney, NSW, Australia; [4]School of Medicine, Deakin University, Geelong, VIC, Australia; [5]Save Sight Institute, Sydney University, Sydney, NSW, Australia

Glaucoma is characterized by the loss of retinal ganglion cells (RGC), and accordingly the preservation of RGCs and their axons has recently attracted significant attention to improve therapeutic outcomes in the disease. Here, we report that Src homology region 2-containing protein tyrosine phosphatase 2 (Shp2) undergoes activation in the RGCs, in animal model of glaucoma as well as in the human glaucoma tissues and that Shp2 dephosphorylates tropomyosin receptor kinase B (TrkB) receptor, leading to reduced BDNF/TrkB neuroprotective survival signaling. This was elucidated by specifically modulating Shp2 expression in the RGCs *in vivo*, using adeno-associated virus serotype 2 (AAV2) constructs. Shp2 upregulation promoted endoplasmic reticulum (ER) stress and apoptosis, along with functional and structural deficits in the inner retina. In contrast, loss of Shp2 decelerated the loss of RGCs, preserved their function, and suppressed ER stress and apoptosis in glaucoma. This report constitutes the first identification of Shp2-mediated TrkB regulatory mechanisms in the RGCs that can become a potential therapeutic target in both glaucoma and other neurodegenerative disorders.

INTRODUCTION

Retinal ganglion cell (RGC) degeneration and optic nerve head (ONH) cupping are characteristic features of glaucoma, which can eventually lead to permanent blindness even when intraocular pressure (IOP)-lowering medications are used. Elevated IOP is the prominent risk factor in primary open-angle glaucoma (POAG), which is the most common form of the disease, but lowering of IOP is not always sufficient to prevent the progression of associated optic neuropathy.[1] Therefore, glaucoma treatment remains open to genetic and pharmacological neuroprotective therapies, in addition to IOP-lowering strategies, to further prevent retinal neuronal loss or delay the disease progression.[2,3]

Several studies have implicated neurotrophins and their receptors, particularly the brain-derived neurotrophin factor-tropomyosin receptor kinase B (BDNF/TrkB) signaling pathway, to play a protective role in the RGCs in glaucoma.[4–7] BDNF is a high-affinity ligand for TrkB, and its ligand-receptor interaction induces TrkB autophosphorylation while promoting phosphatidyl inositol 3 kinase, phospholipase C-γ1, and Erk/mitogen-activated protein kinase (MAPK) pathways.[8–10] While pre-clinical models have made considerable effort in targeting both BDNF and TrkB to orchestrate RGC survival, less is known about the mechanisms that regulate the BDNF/TrkB axis. Intravitreal administration of BDNF or gene therapy targeting BDNF and TrkB has been shown to impart protection to the RGCs in various optic nerve injury models.[6,11,12] However, providing an effective and lasting protection, which translates the beneficial effects of BDNF for therapeutic purposes, has remained elusive. In addition, BDNF is involved in several biological processes and interacts with the p75NTR, N-methyl-D-aspartic acid (NMDA) receptor, and dopamine D3 receptor, leading to non-specific effects.[13–15] This has led to the widely accepted notion that despite the protective effects of targeting BDNF/TrkB signaling, it is not a practical option.

Previous studies have implicated Src homology region 2-containing protein tyrosine phosphatase 2 (Shp2) to negatively regulate TrkB actions in cortical and cerebral neuronal cultures.[16,17] Shp2 is highly expressed in the adult retina and different parts of the brain, including the pituitary gland, olfactory bulb, cerebral cortex, hippocampus, cerebellum, and brain stem.[7,18,19] The tyrosine phosphatase Shp2 is believed to promote receptor tyrosine kinase signaling[20] and plays a critical role in regulating cytoskeleton arrangement, cell differentiation, and division.[21] It has also been shown to be involved in neurotrophic factor signaling and regulate TrkB actions in mesencephalic and cortical neuronal cells.[16,22] Furthermore, the non-receptor phosphatase plays prominent role in several signal transduction cascades,

Received 3 June 2018; accepted 27 September 2018;
https://doi.org/10.1016/j.ymthe.2018.09.019.

Correspondence: Nitin Chitranshi, Faculty of Medicine and Health Sciences, 75 Talavera Road, Macquarie University, Sydney, NSW 2109, Australia.
E-mail: nitin.chitranshi@mq.edu.au
Correspondence: Vivek K. Gupta, Faculty of Medicine and Health Sciences, 75 Talavera Road, Macquarie University, Sydney, NSW 2109, Australia.
E-mail: vivek.gupta@mq.edu.au

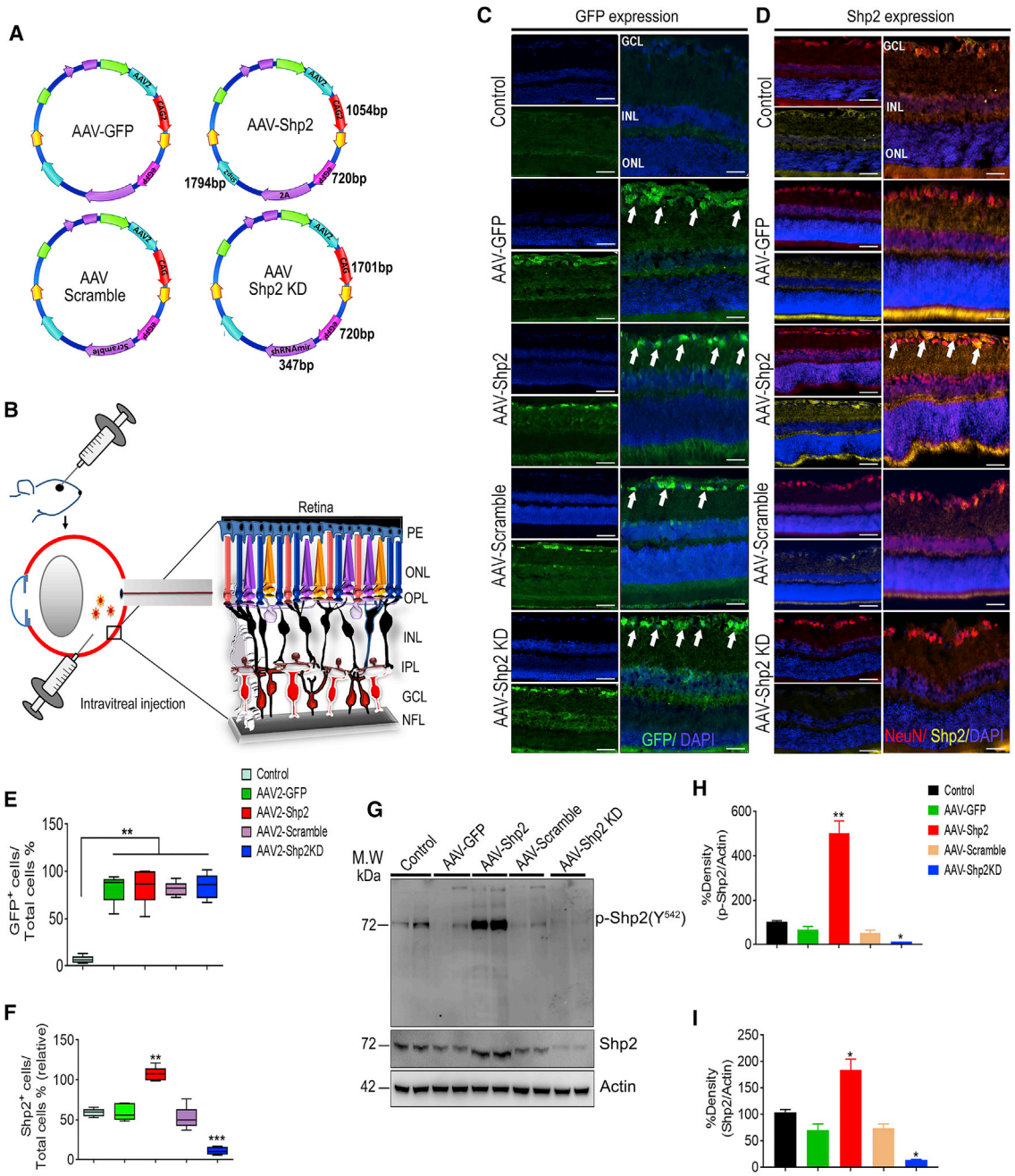

Figure 1. AAV-Mediated Shp2 Expression Modulation in Retinal Ganglion Cells

(A) Map of AAV plasmid vector containing GFP, mShp2, scrambled shRNA, and mShp2shRNAmir sequence. mShp2 (overexpression) and mShp2shRNAmir (KD) sequences were cloned in AAV2 viral vector plasmid fused to the ampicillin-resistance gene. For protein co-expression, a T2A self-cleaving peptide sequence was used in AAV-Shp2 construct only. (B) Schematic representation of intravitreal injection of AAV2-viral constructs in the rat retina. (C and D) Rat eyes were injected with AAV2 constructs for Shp2 overexpression and knockdown. GFP alone or GFP co-expressed with scrambled shRNA sequence were used as controls (final concentration, 3.4×10^{12} GC/mL) as indicated. Retinal sections were stained with DAPI (blue), anti-GFP (green), and anti-Shp2 (yellow) to evaluate expression of GFP (C) and Shp2 (D), respectively, with NeuN (red) as neuronal marker 8 weeks after the AAV2 intravitreal injection. Scale bars, 50 μm. (E) Following intravitreal injection, a significant increase of GFP-positive expression in RGCs was observed compared to control animal eyes (**$p < 0.006$; one-way ANOVA; n = 14 each group). (F) Shp2 expression in the GCL was significantly increased upon intravitreal administration of AAV2-expressing Shp2 and decreased upon Shp2 KD compared to control and AAV2-Scrambled-injected eyes (**$p < 0.005$, ***$p < 0.0004$; one-way ANOVA; n = 14). (G) Lysates of control and AAV-injected ONH were probed with Shp2 and phospho-Shp2 (Y^{542}) using specific antibodies with actin as loading control.

(legend continued on next page)

which are involved in the early development of vertebrates, transcription regulation, and metabolic control.[23–26] Shp2-mediated signaling was also shown to mediate neural cell-fate decisions during development in the CNS and protect against brain injury induced by ischemia.[27,28]

The non-receptor tyrosine phosphatase is constitutively expressed in mature RGCs suggestive of its putative role in normal RGC physiology, which is not completely understood.[7] In the isolated RGCs, TrkB was shown to interact with Shp2 in immuno-precipitation, and this interaction was observed to be mediated through the membrane adaptor protein caveolin.[7] We also observed that Shp2 activity was elevated in the isolated rat RGCs, which were exposed to either chronic or acute optic nerve injury, and this correlated inversely with TrkB activation in these cells. These reports provided a proof-of-principle that TrkB activity in the RGCs may be amenable to sustained upregulation if the partner phosphatase Shp2 is specifically inhibited in these cells, and this in turn could provide a structural and functional phenotypic rescue in glaucoma, where these cells are preferentially affected. Recently, we also provided evidence to support this hypothesis in SH-SY5Y cells by demonstrating that Shp2 silencing promotes TrkB activity and neuritogenesis and, conversely, that phosphatase upregulation antagonizes TrkB phosphorylation and induces endoplasmic reticulum (ER) stress response and apoptotic pathway activation.[29]

Here, we employed adeno-associated virus serotype 2 (AAV2) to modulate the expression of Shp2 in both healthy and glaucomatous retinas to evaluate the *in vivo* interactions between Shp2 and TrkB and delineate the effects of Shp2 modulation on retinal structure and function. The AAV2 used was highly efficient and allowed specific and sustained RGC transduction. This study demonstrated for the first time that sustained *Shp2* upregulation induced RGC degeneration and conversely that genetic silencing of Shp2 in glaucoma rescued the inner retinal degenerative phenotype in the disease. This therapy has the potential to enhance TrkB receptor activation that is typically reduced in the RGCs in glaucoma. Thus, the results provide novel and important data on the therapeutic modulation of Shp2 in rescuing inner retinal impairment in an experimental glaucoma model.

RESULTS

AAV2 Gene Therapy Induces Sustained Transgene Expression in the RGCs

Transgene expression cassettes of EGFP, Shp2, scrambled sequence, and small hairpin RNA (shRNA)mir were administered intravitreally using four different AAV2 viral vectors under the control of CAG2/CAG promoter (Figures 1A and 1B).[30–32] A synthetic linker polyadenylation signal separated the expression of Shp2 sequence from the co-expressing EGFP (Figure S1A). Rat retinas exhibited EGFP expression in the ganglion cell layer (GCL) 2 months following the AAV2 administration, and Shp2 immunostaining of the sections also revealed significantly elevated Shp2 expression in the GCL of retinas administered AAV2-mShp2 while the expression was suppressed in AAV2-Shp2-shRNAmir-transduced retinas (Figures 1C and 1D). The sustained modulation of the phosphatase expression in the GCL 2 months following single intravitreal administration was established using immunofluorescence staining (Figures 1C, 1D, and S1B–S1J), and on an average 80% ± 6% increase in GFP^+ RGCs was observed in AAV2-transduced eyes compared to the control eyes (Figure 1E). Shp2 staining revealed around 2-fold upregulation in the protein expression in GCL compared to control and EGFP alone expressing retinas while a 5.45- ± 2-fold decrease in Shp2 expression was identified in the GCL of rat eyes subjected to AAV2-mediated Shp2 silencing (Figure 1F). NeuN staining was used as a ganglion cell marker to co-localize EGFP and Shp2 expression in the retina (Figures S1C–S1J). Further, staining with the GFP and Shp2 revealed co-localization of Shp2 in GFP^+ RGCs (Figure S2). The transgene expression modulation was also validated using immunoblotting analysis of the ONH of the rat retinas. Elevated Shp2 expression (1.8- ± 4-fold) was observed in the retinas subjected to AAV2-Shp2 transduction, while the expression was downregulated in AAV2-Shp2 shRNAmir (7.4- ± 4-fold)-transduced eyes (Figure 1G). p-Shp2 Y^{542} immunoblotting established increased staining in the group subjected to Shp2 overexpression, indicating that the phosphatase was biologically active (Figure 1G). Densitometric quantification of the band intensities revealed 4.9- ± 3-fold increased p-Shp2 Y^{542} in overexpression eyes and 2- ± 3-fold downregulation in Shp2 knockdown (KD) tissues compared to the control retinas (Figures 1H and 1I).

Shp2 Regulates TrkB Signaling in the RGCs

To evaluate the contribution of Shp2 expression modulation on TrkB phosphorylation and its downstream signaling on the RGCs, we subjected the rat retinal sections to TrkB and p-TrkB Y^{515} staining (Figures 2A and S3). Corroborating the previous evidence of Shp2-mediated regulation of TrkB actions,[7] we observed that *Shp2* upregulation resulted in reduced TrkB (Y^{515}) phosphorylation in the GCL (Figure 2A). Conversely, *Shp2* KD led to increased (Y^{515}) phosphorylation of TrkB compared to the control retinas in the GCL *in vivo* (Figure 2A). TrkB represents the high-affinity receptor for BDNF for supporting long-term RGC survival.[33] Analysis of BDNF/TrkB signaling, accordingly, represents a useful tool for identifying the likely cell-survival signaling pathway of Shp2 gene therapy. In control AAV-GFP and AAV-Scrambled transduced eyes, basal levels of p-TrkB (Y^{515}) were detectable (Figure 2A). To confirm that TrkB activation within the GCL, principally reflected neuronal cell population, double labeling of sections with anti-βIII tubulin or NeuN was

(H and I) Relative changes in band intensities of p-Shp2 and Shp2 were quantified and plotted, indicating upregulation of p-Shp2 (H) and Shp2 (I) levels (*$p < 0.05$, **$p < 0.009$; one-way ANOVA; n = 14). Data are represented as mean ± SD. AAV2, adeno-associated virus, serotype 2; CAG, cytomegalovirus (CMV) chicken β-actin rabbit beta-globin gene; EGFP, enhanced green fluorescence protein; Shp2, Src homology region 2-containing protein tyrosine phosphatase 2; shRNAmir, short hairpin RNA; GCL, ganglion cell layer; INL, inner nuclear layer; ONL, outer nuclear layer. See also Figures S1 and S2.

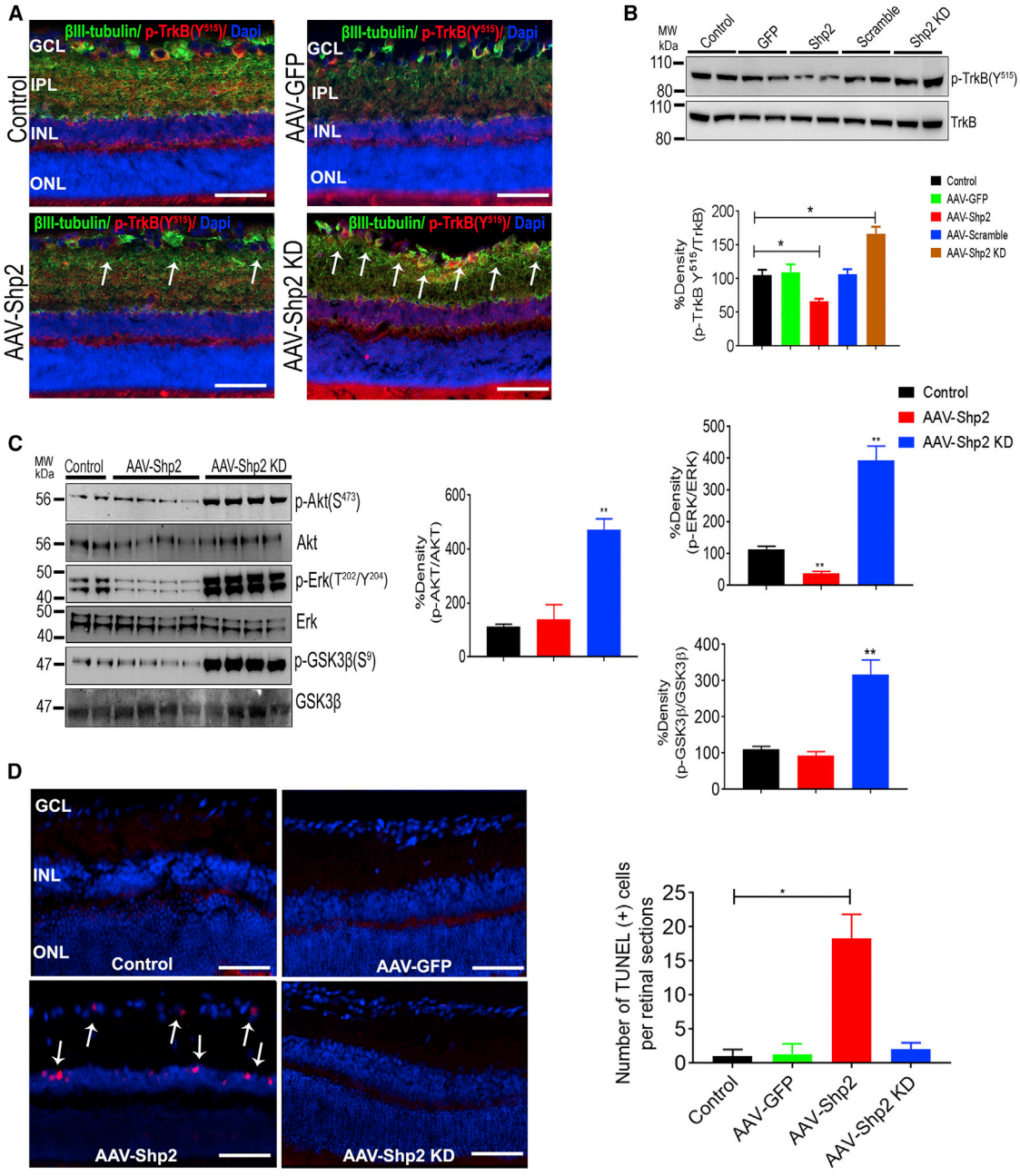

Figure 2. Shp2 Upregulation Negatively Affects TrkB Signaling and Promotes Apoptosis in the Inner Retina

(A) Shp2 expression modulated and control retinal sections were double-labeled with βIII-tubulin (green), and p-TrkB Y^{515} (red) antibodies. Co-localization of p-TrkB Y^{515} and βIII-tubulin in the GCL is indicated by arrows (white). DAPI (blue) used to stain nuclei. Scale bars, 50 μm. (B) Western blot analysis of ONH lysates from control and AAV-injected eyes demonstrated reduced phospho-TrkB Y^{515} levels upon Shp2 overexpression and enhanced p-TrkB Y^{515} AAV-Shp2 KD eyes compared to control samples, 8 weeks post-intravitreal injection (*$p < 0.04$; one-way ANOVA; n = 8 rat per group). (C) Immunoblotting and data quantification indicated that Shp2 overexpression resulted in loss of TrkB downstream signaling in ONH lysates. Shp2 downregulation was associated with Akt (p-Akt S^{473}) and p-Erk ($T^{202/204}$) activation, while its upregulation resulted in suppression of p-Erk ($T^{202/204}$) phosphorylation. Shp2 downregulation also resulted in significant increase in GSK3β (S^{9}) phosphorylation. Total Akt, Erk, and GSK3β proteins were relatively unchanged (**$p < 0.007$; one-way ANOVA; n = 4 rats per group). (D) TUNEL staining of the AAV-modulated and control frozen retinal sections was performed and analyzed using fluorescence microscopy. Increased TUNEL labeling (red) in GCL and INL was observed in Shp2-overexpressing retinas (white arrows). Quantification of TUNEL-positive cells showing significantly increased numbers in AAV-Shp2 overexpression retina compared to control, AAV-GFP, and AAV-Shp2 KD. Data presented as mean ± SD (*$p < 0.03$; one-way ANOVA; n = 4 rats per group). DAPI (blue) was used to reveal tissue architecture. Scale bars, 50 μm. GCL, ganglion cell layer; INL, inner nuclear layer; ONL, outer nuclear layer. See also Figures S3, S4, and S5.

performed (Figures 2A and S4). Immunoblotting of ONH tissue lysates and quantification further validated p-TrkB Y^{515} protein expression alterations in response to AAV transduction (Figure 2B). BDNF localization and expression pattern remained unaffected in Shp2-overexpression- and Shp2-KD-subjected retinas (Figure S5A). We also observed no significant variations in IOP as a consequence of AAV intravitreal injections (Figure S5B). Analysis of TrkB expression in retinal and ONH tissues revealed that there was no compensatory change in total TrkB protein levels in response to AAV transduction or *Shp2* modulation (Figures S3 and 2B), suggesting that loss of (Y^{515}) phosphorylation was mediated through the bona fide phosphatase activity of Shp2. This was in accordance with previous observations that *Shp2* deletion in neuronal cultures reversed TrkB inhibition and promoted neuronal survival.[17]

Since Shp2 has been shown to regulate Akt/Erk/Gsk3β pathways,[8,34,35] we investigated whether tyrosine phosphatase was also involved in regulating these major phosphatidylinositol 3-kinase (PI3K), Ras/MAPK effector pathways of BDNF/TrkB signaling in the inner retina. We observed significant loss of Erk phosphorylation (T^{202}/Y^{204}) in ONH tissues of animals subjected to Shp2 overexpression. BDNF/TrkB signaling has previously been shown to induce Erk activation in hyperglycemic retinal neurons.[36] In contrast, the protein overexpression did not inhibit p-Akt (S^{473}) and p-GSK3β (S^{9}) phosphorylation. Reciprocally, Shp2 silencing resulted in significant enhancement of Akt (S^{473}), Erk (T^{202}/Y^{204}), and GSK3β (S^{9}) phosphorylation, when normalized to the total Akt, Erk, and GSK3β expression (Figure 2C). Taken together, these results implicated that Shp2 negatively modulated the TrkB activity.

Recently, we identified that Shp2-induced cell-growth inhibition, loss of neurite growth, and apoptotic pathway activation in neuroblastoma cells,[29] and loss of BDNF/TrkB signaling is linked with inner retinal degenerative phenotype.[37] We therefore investigated whether sustained Shp2 modulation in the adult RGCs affected their survival. Our results showed significant increased TUNEL-positive cells in the GCL subjected to Shp2 overexpression (Figure 2D). Control, GFP, and scrambled-sequence-transduced retinas were used as normal and AAV-injected corresponding controls (Figure 2D). Shp2-knockdown-subjected retinas revealed no noticeable apoptotic staining in the GCL and were comparable to control and EGFP-alone-transduced retinas.

Shp2 Overexpression Is Detrimental for the Inner Retinal Structural and Functional Integrity

We evaluated whether Shp2 expression modulation could bring any changes in the inner retinal structure or function, particularly in the RGCs. Histopathological and morphometric changes 2 months following Shp2 expression modulation post-AAV2 transduction were analyzed. EGFP and scrambled sequence transduced animals were used as controls. H&E staining revealed a significantly reduced GCL density in the animals that were subjected to Shp2 overexpression in the RGCs, compared to the control eyes (Figures 3A–3C). A 2-fold reduction in GCL density was observed over a 2-month time frame (Figure 3B). No significant retinal laminar structural changes were identifiable in other retinal layers, in any of the experimental groups. We also used NeuN, a neuronal marker, to quantify RGCs after AAV intravitreal injection. Quantification of NeuN-labeled cells showed significant decrease in $NeuN^{+}$ cells in animals overexpressing Shp2 compared to healthy and other AAV-injected eyes (Figure S6) (***$p < 0.0001$, one-way ANOVA, Bonferroni post-hoc test; $n = 3$, control 30.29 ± 0.74 versus AAV-Shp2 13.48 ± 0.73 $NeuN^{+}$ cells). To further assess the RGC loss, we analyzed the axonal integrity of the optic nerve, using para-phenyldiamine (PPD) staining. An increase in the incidence of degenerative axon profiles and vacuolization was observed in the extra-axonal space following Shp2 overexpression over a period of 2 months (Figure 3D). Quantification of degenerative profiles revealed that the number of degenerative axon profiles increased 2.2-fold on average in Shp2-treated optic nerves compared with control and GFP-, scrambled-, and Shp2-treated optic nerves (**$p < 0.002$; one-way ANOVA, Bonferroni post-hoc test; $n = 3$; Figure 3E). However, Bielchowsky's silver staining also showed significant reduction in optic nerve axonal density in animals subjected to *Shp2* overexpression (Figure S7). Similar to retinal structure morphology, optic nerve axons were also well preserved in EGFP control and scrambled-sequence-transduced animals. No significant changes were observed in the retinas and optic nerves of animals subjected to Shp2 silencing (Figures 3D and 3E), suggesting that constitutive Shp2 expression in adult retinas was not absolutely essential for inner retinal structure and function.

We then investigated whether inner retinal structural deficits were linked with any functional losses upon Shp2 modulation. Electrophysiology recordings (ERGs) and positive scotopic threshold response (pSTR) measurements were carried out 2 months following Shp2 modulation. Significant reduction in pSTR amplitudes (44% ± 3.1%) in AAV-Shp2 transduced eyes was observed compared to the EGFP control eyes (Figures 3F and 3G). No significant changes in pSTR amplitude were observed in scrambled or Shp2-shRNAmir-transduced eyes (Figures 3H and 3I). Whole retinal scotopic ERG further demonstrated no significant changes in the waveform or amplitudes in any of the Shp2 modulation or control groups, although a slight reduction in b-wave amplitudes was observed in AAV-Shp2-overexpression eyes (Figures 3J–3M). Together, our retinal and optic nerve structural and functional data implicated that sustained upregulation of Shp2 in the RGCs promoted inner retinal degenerative changes. These adult retinas, in contrast, were resilient when subjected to KD of the constitutive expression of the Shp2 protein.

TrkB Signaling Is Restored in the Glaucoma Retinas upon Shp2 Silencing

We previously reported increased Shp2-TrkB interactions in the RGCs isolated from rat retinas using immunoprecipitations.[7] In this study, we identified that Shp2 expression and TrkB downstream signaling proteins are affected in human post-mortem glaucoma retinas (Figure 4). Immunohistochemistry of human control and glaucoma retinas showed increased pShp2 Y^{542} staining in the inner retinas from glaucoma subjects compared to the control tissues

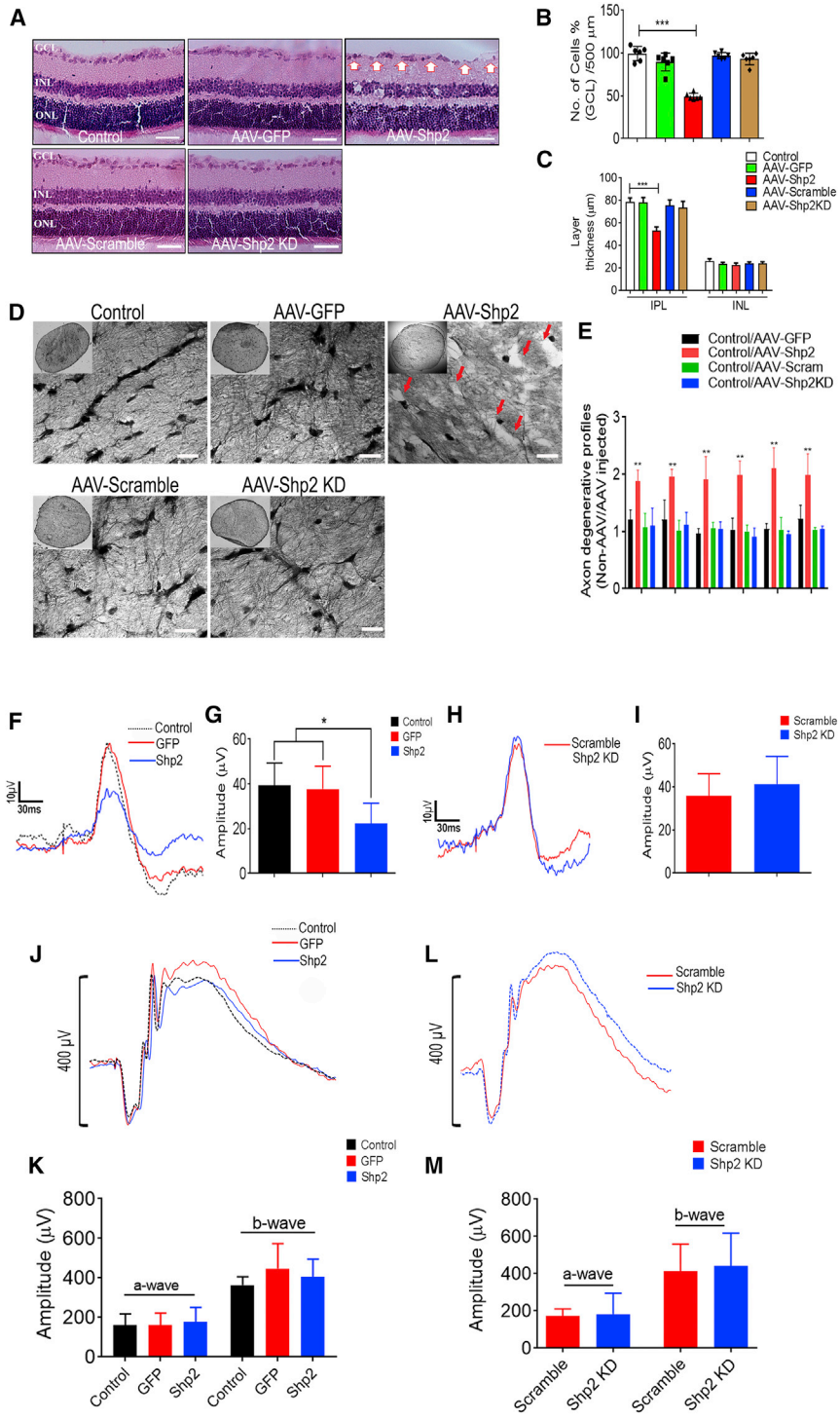

Figure 3. Impairment of Inner Retinal Structure and Function upon Shp2 Overexpression

(A) H&E staining of Shp2-modulated and control retinas after 8 weeks of AAV2 administration revealed reduced GCL density (white arrow) and IPL thickness. No significant retinal laminar structural changes were observed in eyes expressing GFP, scrambled, and Shp2 KD sequence compared to control eyes. Scale bars, 50 µm. (B and C) Quantification revealed significantly reduced GCL density (B) and IPL thickness (C) in Shp2-overexpressing retinas (***$p < 0.0006$, one-way ANOVA; n = 4 rats per group). No significant changes were observed in INL thickness between control and AAV2-administered eyes. (D) PPD staining was performed on cross-sections of rat optic nerves to assess changes in optic nerve axons upon Shp2 expression changes. The cross-sections show that astrocytes and neural fibers are arranged evenly in control and GFP-, scrambled-, and Shp2 KD-treated animals. Shp2 overexpression in the animal retina results into disappearance of the cylindrical arrangement of astrocytes completely, and vacuoles were observed in the damaged area (shown with red arrow) (scale bars, 10 µm). (E) More degenerating profiles were observed in optic nerve cross-sections in Shp2-treated compared with untreated, GFP, scrambled, and Shp2 KD eyes (**$p < 0.002$, one-way ANOVA; n = 3 rats per group). (F) Average positive scotopic threshold response (p-STR) traces of control and AAV-GFP- and AAV-Shp2-administered retinas. (G) Quantification revealed reduced p-STR amplitudes following 8 weeks of Shp2 overexpression (*$p < 0.05$, one-way ANOVA; n = 14 rats per group). (H) Average p-STR responses of control and Shp2 eyes. (I) Quantification indicated no significant reduction in p-STR amplitudes upon Shp2 KD (n = 14 rats per group). (J) Average electroretinogram (ERG) of Shp2-overexpressing, GFP, and control eyes of SD rats. (K) Data analyses of ERG a- and b-wave amplitudes revealed no significant differences between groups (n = 14 rats per group). (L) Average ERG of SD rats expressing scrambled and Shp2 KD sequences also revealed (M) no significant changes among Shp2 KD and scrambled sequence groups (n = 14 rats per group). Data are represented as mean ± SD. GCL, ganglion cell layer; INL, inner nuclear layer; IPL, inner plexiform layer; ONL, outer nuclear layer. See also Figures S6 and S7.

(Figures 4A and 4B). In contrast, a prominent reduction of pTrkB Y^{515} was identified in retinas from glaucoma subjects (Figures 4C and 4D). Immunostaining with βIII-tubulin showed localization of both of these proteins within the RGCs (Figures 4A–4D). Western blotting results further demonstrated increased pShp2 Y^{542} and decreased pTrkB Y^{515} immunoreactivity in the ONH tissues from glaucoma samples, in agreement with immunohistochemistry analysis. There was also an increased Shp2 expression observed in glaucoma tissues, while no significant changes were observed in the total TrkB levels, indicating receptor dephosphorylation (Figures 4E–4H). The TrkB downstream PI3K, Ras/MAPK, and GSK3β signaling changes were analyzed in the ONH lysates from glaucoma samples. Significant reduction in pAkt (S^{473}) (Figures 4I and 4J), pErk (T^{202}/Y^{204}) (Figures 4K and 4L), and pGsk3β (S^{9})

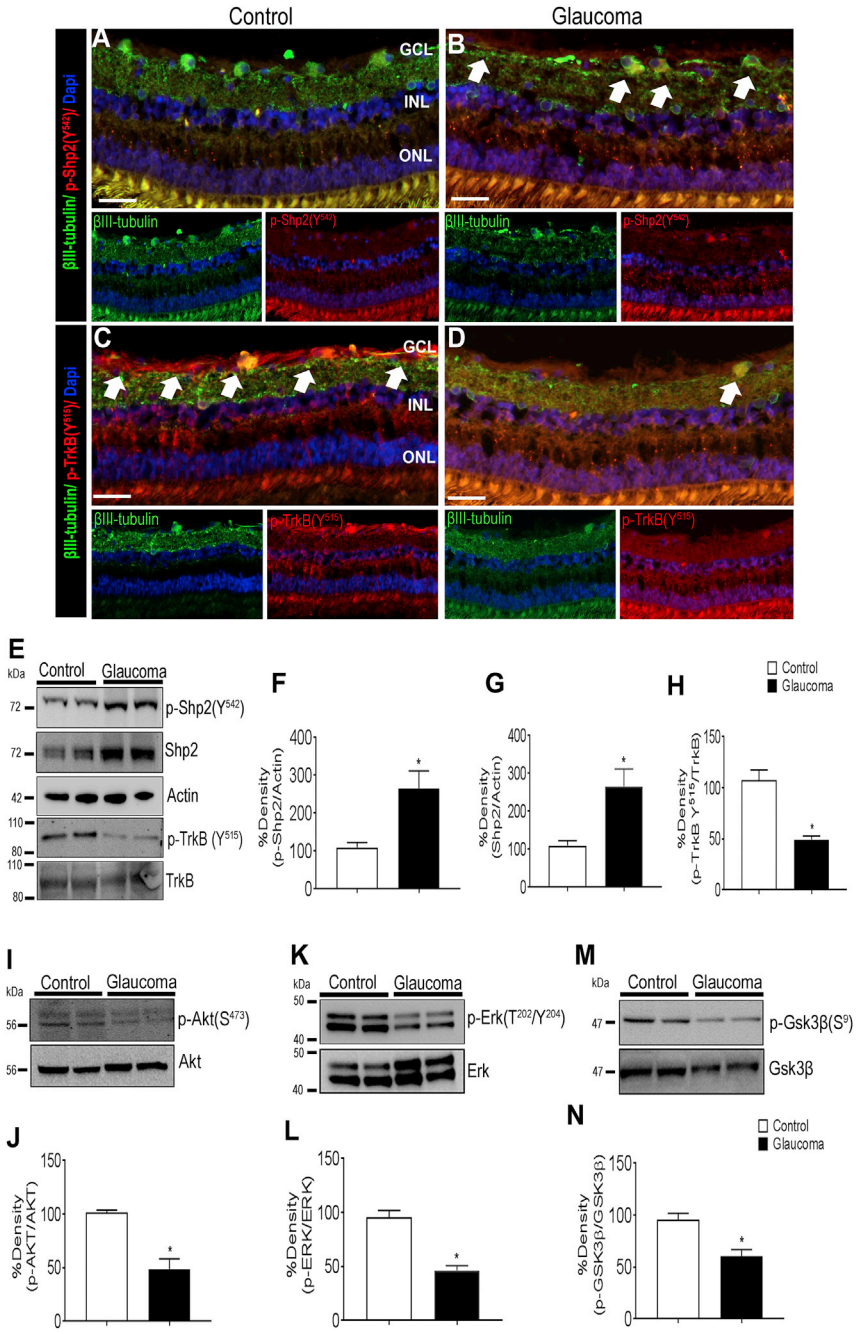

Figure 4. Increased Shp2 and Loss of TrkB Activation in Human Glaucoma Retinas

(A and B) Human retinal sections probed for phospho-Shp2 (Y^{542}) (red) revealed increased staining in (B) glaucoma tissues (arrow) compared to (A) control ones (βIII-tubulin, green). (C and D) In contrast, probing for TrkB (Y^{515}) indicated higher staining in the control retinas (arrow) compared to the tissues from glaucoma subjects. Nuclei were counterstained with DAPI (blue). Scale bars, 50 μm. (E) Western blot of ONH lysates probed for phospho-Shp2 (Y^{542}), Shp2, phospho-TrkB (Y^{515}), and TrkB. (F) Quantification of band intensities revealed significant increase in expression of p-Shp2 (Y^{542}) in glaucoma (*$p < 0.04$; Student's t test; n = 3 human eyes per group). (G) Significant increase in expression of Shp2 (*$p < 0.05$; Student's t test; n = 3 human eyes per group) and (H) decrease in phospho TrkB (Y^{515}) was observed in human glaucoma ON lysates (*$p < 0.02$; Student's t test; n = 3 human eyes per group). (I) Western blot of ONH lysates showing expression of pAkt (S473) and Akt in control and glaucoma human subjects. (J) Quantification of band intensities revealed significant loss of pAkt (S^{473}) levels in glaucoma (*$p < 0.02$; Student t test; n = 3 human eyes per group). (K) Western blot of ONH lysates showing expression of p-Erk (T^{202}/Y^{204}) and Erk in control and glaucoma human subjects. (L) Quantification of band intensities revealed significant loss of p-Erk (T^{202}/Y^{204}) levels in glaucoma (*$p < 0.01$; Student's t test; n = 3 human eyes per group). (M) Western blot of ONH lysates showing expression of p-Gsk3β (S9) and Gsk3β in control and glaucoma human subjects. (N) Quantification of band intensities revealed significant reduction in p-Gsk3β (S^{9}) phosphorylation levels in glaucoma (*$p < 0.03$; Student's t test; n = 3 human eyes per group). Data are represented as mean ± SD. GCL, ganglion cell layer; INL, inner nuclear layer; ONL, outer nuclear layer.

(Figures 4M and 4N) were observed compared to the control tissues, indicating these survival pathways were negatively affected in glaucoma. No significant changes were observed in the total Akt, Erk1/2, and GSK3β proteins.

The correlation between increased Shp2 activity and loss of TrkB signaling was investigated in the animal model of glaucoma that was further subjected to Shp2 silencing. Following sustained chronic IOP elevation for 2 months, the GCL demonstrated reduced pTrkB Y^{515} and elevated pShp2 Y^{542} immunostaining. Remarkably, the glaucoma animals that were further subjected to Shp2 silencing showed increased pTrkB Y^{515} staining in the GCL, implicating that TrkB phosphorylation in the RGCs was being inversely regulated by Shp2 under glaucomatous conditions (Figures 5A and 5B). βIII-tubulin staining was used to determine the localization of pTrkB Y^{515} and pShp2 Y^{542} to the GCL. We also evaluated the changes in pTrkB Y^{515} and pShp2 Y^{542} in the glaucomatous eyes using ONH tissue lysates and the results validated the immunohistochemistry findings. A significant reduction in pTrkB Y^{515} was observed in high-IOP tissue lysates that was restored upon Shp2 silencing (Figures S8A and S8B). On the other hand, high-IOP exposed ONH tissue lysates showed upregulation of Shp2 and a correspondingly increased pShp2 Y^{542} phosphorylation, which was reduced upon Shp2 silencing using Shp2-shRNAmir transduction (Figures 5C–5E). Corresponding to that observed in human glaucoma samples, a significant downregulation of Akt (S^{473}), Erk ($T^{202/Y204}$), and GSK3β (S^{9}) was observed in the rat ONH tissue.

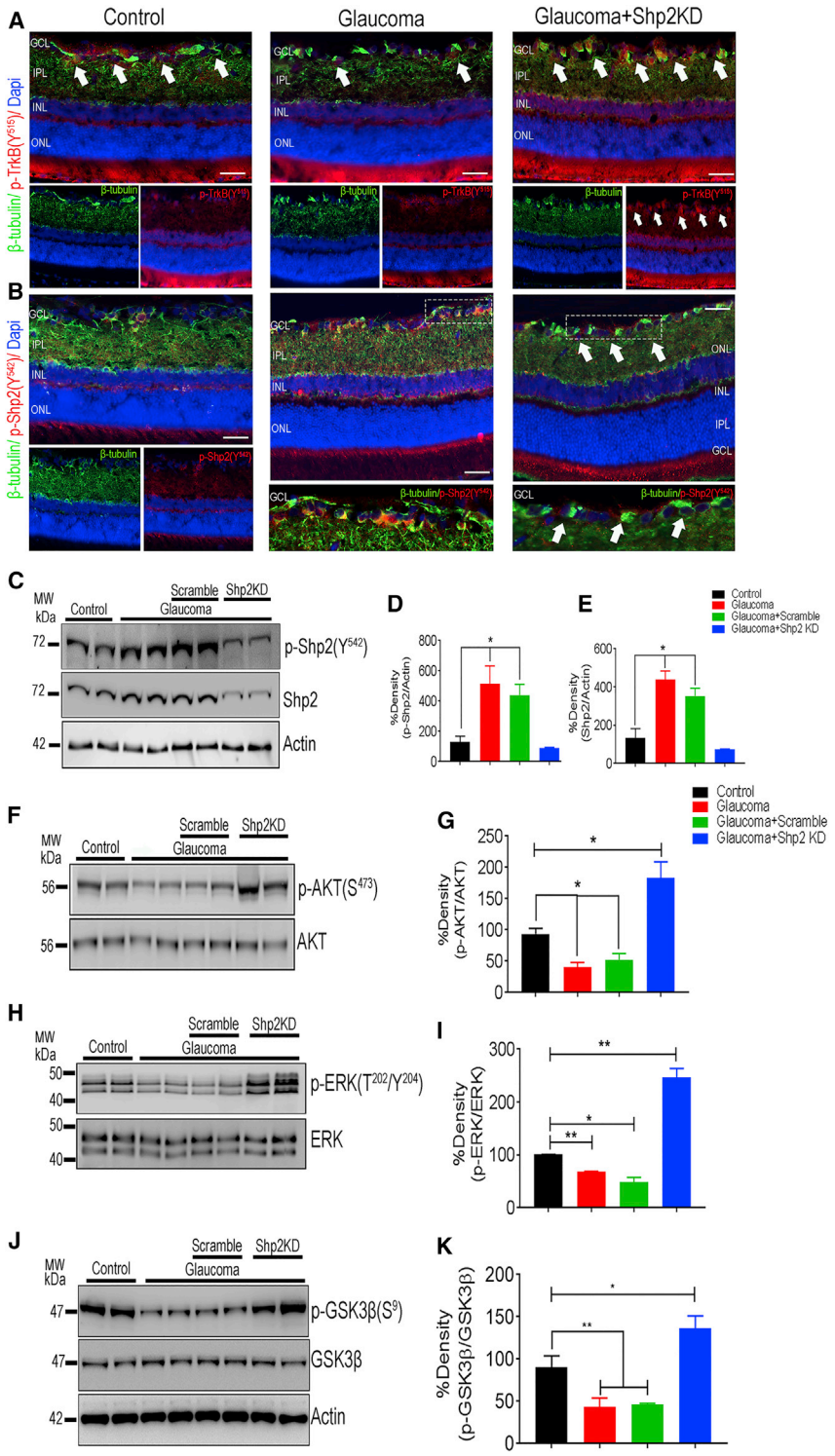

Figure 5. Shp2 Silencing Promotes TrkB Signaling in Glaucoma Model

(A) Decreased phospho-TrkB (Y^{515}) (red) levels were identifiable in βIII-tubulin (green)-positive RGCs in rat retinas subjected to increased IOP, compared to the control eyes (arrow). Shp2 silencing in glaucoma animals rescued the TrkB deactivation. (B) Increased IOP retinal sections revealed higher p-Shp2 (Y^{542}) staining (red) that was prominently diminished upon Shp2 KD (arrows). Nuclei were counterstained with DAPI (blue). Scale bars, 50 μm. (C) Western blot showing p-Shp2 (Y^{542}) and Shp2 expression in high IOP ONH tissue lysates under control and Shp2 KD conditions. (D and E) Densitometric quantification of immunoblots showed significant increase in (D) p-Shp2 (Y^{542}) (*$p < 0.05$; one-way ANOVA; n = 4) and (E) Shp2 protein levels (*$p < 0.03$; one-way ANOVA; n = 4 rats per group) in increased IOP (*$p < 0.05$; n = 4) conditions. Actin was used as loading control. (F and G) Representative western blot (F) and quantification of p-Akt (S^{473}) and Akt levels (G) in experimental glaucoma conditions with and without Shp2 silencing (*$p < 0.05$; one-way ANOVA; n = 4). (H and I) Western blotting (H) and data quantification of p-Erk (T^{202}/Y^{204}) and total Erk levels (I) (*$p < 0.02$, **$p < 0.008$; one-way ANOVA; n = 4). (J and K) Representative western blot (J) and quantification of p-GSK3β (S^{9}) and GSK3β levels (K) in experimental glaucoma conditions with and without Shp2 silencing (*$p < 0.05$, **$p < 0.004$; one-way ANOVA; n = 4) with actin as loading control. Data are represented as mean ± SD. GCL, ganglion cell layer; INL, inner nuclear layer; ONL, outer nuclear layer. See also Figures S8 and S9.

Retinas subjected to AAV2-mediated Shp2 silencing showed remarkable protection of these major TrkB downstream survival signaling pathways (Figures 5F–5K). Densitometric analysis confirmed that Shp2 KD-subjected tissues led to a 1.9- ± 2-fold increase in phospho-Akt, 2.5- ± 0.5-fold increase in phospho-Erk, and around 1.5-fold increase in phospho-GSK3β levels compared to the control retinas (Figure 5G, 5I, and 5K). We also evaluated global proteome changes in the retina in response to Shp2 KD and identified 1,579 non-redundant proteins across Shp2 KD and scrambled-sequence-transduced retinas exposed to the high IOP (Data S1).

Exposure to experimental glaucoma resulted in downregulation of 219 and upregulation of 73 proteins in the retina. Data analysis indicated that differentially regulated proteins included the ones that are associated with intracellular signal transduction, metabolic processes, and cellular response to oxidative stress. Computational analysis indicated that proteins associated with MAP kinase activity and Ras signaling were upregulated in Shp2-KD-subjected animal retinas compared to the scrambled-sequence-transduced eyes (Figure S9). Further, decreased expression of crystallins has previously been reported in various models of glaucomatous neurodegeneration, and we recently observed decreased crystallin

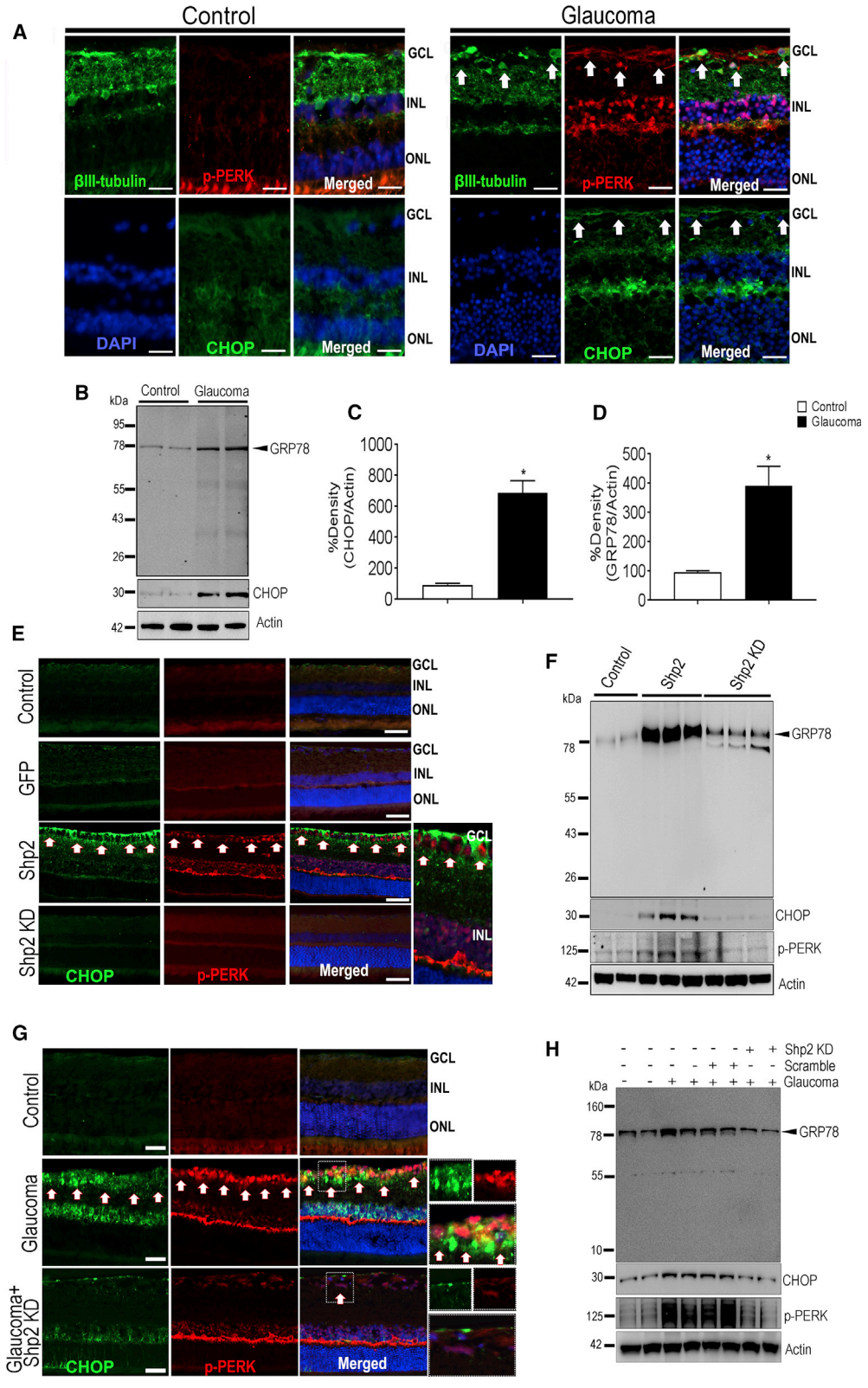

(legend on next page)

levels in samples from human glaucoma subjects.[38–40] Studies have shown enhanced survival of stressed RGC in retinas overexpressing alpha A or alpha B crystallins.[38] Corroborating these observations, Shp2 downregulation resulted in enhanced levels of several crystallin proteins (Cryaa, Cryab, Crybb1, Crybb2, Crybb3, Cryba1, Crygs, and Cryba4) in the glaucomatous retinas (Figure S5; Data S1). A complete list of the proteins identified in this study and their differential regulation is included in Data S1. In brief, these results indicated that Shp2 silencing in RGCs in glaucomatous retinas using gene therapy approach not only restored TrkB activity but also promoted downstream PI3K and MAPK pathways in adult RGCs *in vivo*.

ER Stress in Glaucoma Retinas Is Suppressed upon Shp2 Silencing

To investigate the mechanisms underlying Shp2 modulation effects on the retina, we analyzed the ER stress-associated changes in the human glaucoma retinas and animal retinas exposed to chronically increased IOP. Previous studies have shown that modulating ER-stress pathways has the potential to impart protection against neurodegenerative changes linked with glaucoma.[41] Grp78 regulates the ER-stress-induced unfolded protein response signaling via formation of complex with other proteins present in ER lumen (PKR-like ER kinase [PERK], IRE1α, etc).[29] Grp78 remains bound to PERK in normal physiological conditions, but under stress, Grp78 dissociates and PERK undergoes activation through autophosphorylation.[42] Immunostaining of human retinal sections with ER stress markers CHOP and phospho-PERK (p-PERK) revealed increased staining in the GCL and INL retinal layers (Figure 6A). Western blotting of the human ONH tissues also demonstrated significantly increased GRP78 and CHOP antibody reactivity, confirming increased ER stress in the human glaucoma tissues (Figure 6B). Actin was used as internal loading control for densitometric quantification (Figures 6C and 6D). Our results corroborate previous reports indicating increased ER stress response under glaucoma conditions.[43] To analyze whether increased levels of Shp2 in RGCs influence ER stress response activation, we analyzed the retinas of animals exposed to either Shp2 overexpression or KD using CHOP and p-PERK immunostaining. CHOP-positive cells were distributed predominantly in the GCL, and increased p-PERK immunoreactivity was observed in the GCL and INL, 2 months following AAV-Shp2 transduction (Figure 6E). In contrast, Shp2-KD-subjected eyes were comparable in CHOP and p-PERK immunoreactivity to that of the control and GFP-transduced retinas (Figure 6E). Western blotting and densitometric quantification of the ONH lysates using GRP78, CHOP, and p-PERK antibodies demonstrated significant elevation of these ER stress markers upon Shp2 overexpression, while no remarkable differences were observed in the ER stress markers in the retinal tissues subjected to Shp2 KD (Figures 6F and S10A–S10C). These data indicated that whereas *Shp2* upregulation contributed to enhanced ER stress and cell apoptosis (Figure 2D), the response was not dependent on the loss of endogenous levels of Shp2.

We further examined ER stress-marker changes in our animal model of chronically increased IOP and evaluated the impact of Shp2 KD on the ER stress response on the retina. Consistent with glaucoma human retinal tissues, high IOP exposure for 2 months resulted in elevated CHOP and p-PERK staining in the GCL and INL of the rat retinas, while Shp2 silencing in the high-IOP-exposed retinas lead to marked downregulation of the CHOP and p-PERK immunoreactivity (Figure 6G). Similar results were observed in ONH immunoblotting, where we observed increased GRP78, CHOP, and p-PERK expression under glaucomatous conditions while Shp2 silencing under high-IOP conditions resulted in reduced expression of these markers. Scrambled-sequence-expressing retinas demonstrated no noticeable ER-stress-marker changes compared to the control eyes (Figures 6H and S10D–S10F). These results indicated that suppressing Shp2 expression rescued TrkB signaling and protected against ER stress response in glaucoma.

Restoration of Retinal Structure and Function in Glaucoma

To investigate whether improved BDNF/TrkB signaling and protection against ER stress translated into rescue of inner retinal structural and functional deficits associated with experimental glaucoma, we analyzed the retinal sections using H&E staining. Significant loss of GCL density was observed in the rat retinas exposed to chronically increased IOP for 2 months. The IOP changes ranged from 9.32 ± 0.17 mm Hg for control and 20.84 ± 1.65 mm Hg for the microbead administered animals (Figures 7A–7E and S11A). AAV2-mediated sustained Shp2 silencing in the adult retinas significantly protected the GCL, and cell loss was reduced from 55% ± 2% to 27% ± 3% (Figures 7D and 7E). Retinas expressing scrambled sequence were used as control and exhibited GCL density similar to that observed in high-IOP-exposed eyes alone (Figures 7A–7E). Histological analysis revealed no changes in IPL and INL thickness in any of the treatment groups (Figure 7F). No significant change in GFP expression in the glaucoma and glaucoma + scrambled groups may be attributed to

Figure 6. Shp2 Regulates ER Stress in the Inner Retina in Healthy and Glaucoma Conditions

(A) Increased immunofluorescence staining of ER stress markers CHOP (green) and p-PERK (red) in the RGC layer (arrow) in human glaucoma retinal sections. RGCs and nuclei were counter stained with βIII-tubulin (green) and DAPI (blue), respectively. (B) Western blot analysis of GRP78 and CHOP ER stress protein markers in human ONH lysates. (C and D) Densitometry quantification showed significant increase in expression of Grp78 (D) (*$p < 0.02$; Student's t test; n = 3 human eyes per group) and CHOP (C) (*$p < 0.009$; Student's t test; n = 3 human eyes per group). (E) Increased immunofluorescence staining of ER stress markers CHOP (green) and p-PERK (red) in the GCL (arrow) of animal retinas overexpressing Shp2. Normal expression of CHOP and p-PERK was observed in retinas subjected to control, GFP, and Shp2 KD transduction. (F) Western blot analysis of GRP78, CHOP, and p-PERK in ONH lysates expressing Shp2 and Shp2 KD sequences. (G) Increased immunofluorescence staining of ER stress markers CHOP (green) and p-PERK (red) in the GCL (arrow) of high-IOP eyes that was decreased in Shp2 KD retinas. Higher magnification of RGC layers are shown in right side using single and merged channel. Nuclei were counterstained with DAPI (blue). Scale bars, 50 μm. (H) Immunoblotting of GRP78, CHOP, and p-PERK in ONH tissue lysates of animals subjected to increased IOP without and with Shp2 silencing. Actin was used as loading control. GCL, ganglion cell layer; INL, inner nuclear layer; ONL, outer nuclear layer. See also Figure S10.

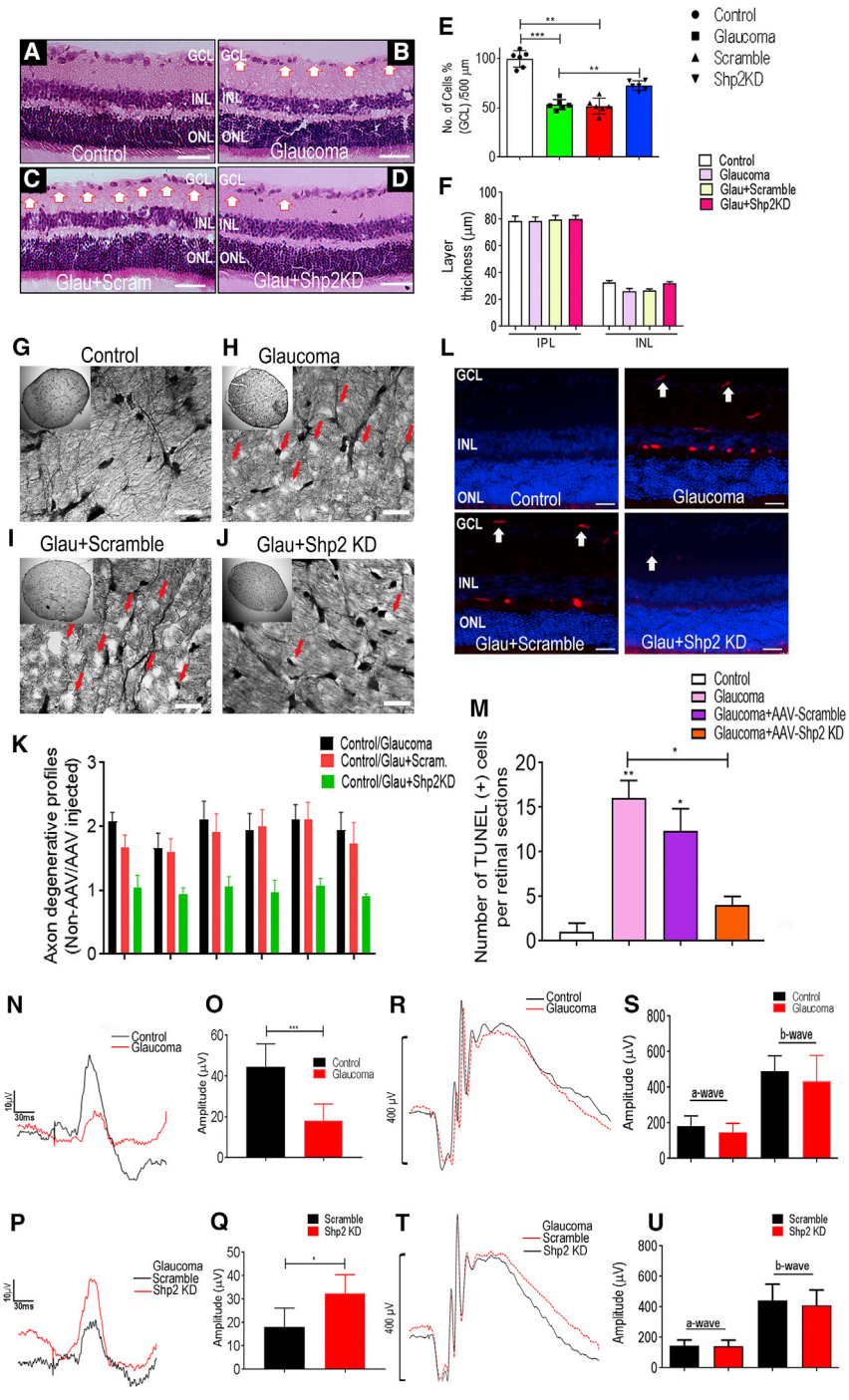

Figure 7. Shp2 Suppression Protects Inner Retinal Structure and Function in Glaucoma

(A–D) H&E staining of control (A), microbead-injected high-IOP (B), high-IOP expressing scrambled sequence (C), and high-IOP (D) retinas subjected to Shp2 silencing. Shp2 silencing revealed protection against GCL thinning induced by high IOP exposure (arrows). Scale bars, 50 µm. (E) GCL thinning in high-IOP-induced retinas (**p < 0.004, ***p < 0.0006; one-way ANOVA; n = 8 rats per group) was significantly reduced in high-IOP animals subjected to Shp2 silencing using AAV2. (F) INL and IPL thickness was measured 500 µm from either side of ONH region. No change in IPL and INL was observed. (G–J) PPD staining for optic nerve axons under control (G), high IOP (H), and high-IOP animals subjected to either scrambled sequence expression (I) or Shp2shRNA (J) (imaged at 63×). The cross-sections show that astrocyte and neural fiber arrangement were disappeared, and vacuoles were observed in the damaged area (red arrow) both in glaucoma and scrambled injection in glaucoma eyes. Shp2 shRNA treatment in glaucoma causes less damage to the astrocytes and neural fiber arrangements (scale bars, 10 µm). (K) More axonal degenerating profiles were observed in optic nerve cross-sections in glaucoma and scrambled injection in glaucoma eyes (p = ns; one-way ANOVA; n = 3; Figure 7K). Shp2shRNA significantly protect glaucomatous axonal degenerative profiles (***p < 0.0003; one-way ANOVA; n = 3). (L) Increased TUNEL-positive staining was observed in retinal sections exposed to microbead injections, and Shp2 silencing lead to reduced TUNEL staining (red) in the inner retinal layers (white arrows). DAPI-stained cell nuclei (blue). Scale bars, 50 µm. (M) Quantification of TUNEL-positive cells showing significantly increased number in glaucoma and glaucoma + AAV-Scamble-injected retina compared to control. Shp2 KD in experimental glaucoma model lead to significant reduction in TUNEL-positive cells in the inner retina (*p < 0.05, **p < 0.009; one-way ANOVA; n = 4 in each group). (N and O) pSTR responses of control and experimental glaucoma animal eyes (N) and a significant decline in p-STR amplitude in the experimental glaucoma animal eyes was observed compared to control after 8 weeks of multiple microbead injections (***p < 0.0004; Student's t test; n = 8) (O). (P and Q) pSTR responses from eyes of scrambled and Shp2 KD-expressing AAV2 sequences in microbead-injected animal eyes (P) and quantification of pSTR amplitude showed significant neuroprotection in the inner retinal function after 8 weeks of animal eyes expressing Shp2 KD sequence under high-IOP conditions (*p < 0.05; Student's t test; n = 8 per group) (Q). (R and S) Average ERG traces of SD rats exposed to high IOP and compared to control recordings (R) and data quantified for a- and b-wave amplitudes (n = 8 rats per group) (S). (T and U) No change in average ERG traces was observed in SD rats expressing scrambled and Shp2 KD sequence under high-IOP conditions (T) and data quantified for a-wave and b-wave amplitudes (n = 8 rats per group) (U). Data are represented as mean ± SD. GCL, ganglion cell layer; INL, inner nuclear layer; ONL, outer nuclear layer. See also Figures S11–S15.

some non-specific expression of the GFP in cells other than the RGCs in the inner retina (Figures S11B and S11C). However, a significant reduction in expression of one of the GFP band was observed in the ONH lysates in the glaucoma + AAV-Scrambled group compared to glaucoma + Shp2-KD-subjected eyes (**$p < 0.007$; one-way ANOVA, Bonferroni post-hoc test; n = 4; Figures S11B and S11D). Anti-NeuN immunostaining showed that $NeuN^+$ cells were significantly reduced in glaucoma and glaucoma + AAV scrambled compared to control and glaucoma+AAV-Shp2 KD (control 30.52 ± 0.27, glaucoma 14.1 ± 0.45, glaucoma+AAV-Scrambled 13.33 ± 0.65, glaucoma + AAV-Shp2 KD 23.76 ± 0.988 $NeuN^+$ cells; ***$p < 0.0009$; one-way ANOVA, Bonferroni post-hoc test; n = 3; Figure S12). Shp2 immunostaining indicated that Shp2 expression was markedly reduced 2 months after Shp2 silencing compared to the high-IOP-exposed eyes (Figure S13A–S13D).

RGC axons converge at the optic nerve, and therefore we tested the protective effects of Shp2 silencing on the optic-nerve axons using PPD and Bielchowsky's silver staining. Similar to the observations of cellular degeneration in GCL, optic nerve degenerative axon profiles were increased in experimental glaucoma or AAV-Scrambled-exposed tissues (Figures 7G–7I). The cylindrical arrangement of astrocytes disappeared after 2 months in optic nerve cross-section of animals exposed to high IOP and scrambled injection in high-IOP model. Several vacuoles of different sizes, demyelination of the nerve, and uncovered axons were observed in these groups of animals (Figures 7H and 7I). By contrast, KD of Shp2 in glaucomatous RGCs led to better organization of the optic nerve cytoarchitecture, which was followed by noticeable preservation of nerve fibers and less disappearance of the astrocyte's cylindrical arrangement (Figure 7J and S14A). Quantification of degenerative profiles revealed that the number of degenerative axon profiles increased 2.3-fold on average in glaucoma alone and glaucoma + scrambled-injected optic nerves compared with optic nerve subjected to Shp2 KD (Figure 7K). However, Bielchowsky's silver staining also showed significant reduction in optic nerve axonal density in animals subjected to *Shp2* overexpression (Figure S14). Axonal degenerative profiles and axonal loss was significantly reduced in AAV-Shp2-shRNAmir transduced group after 2 months (Figures 7J, 7K, and S14; ***$p < 0.0003$, one-way ANOVA, Bonferroni post-hoc test; n = 3), thereby further validating that Shp2 silencing protected the RGCs under glaucomatous conditions.

Sustained exposure to chronically increased IOP-induced TUNEL-positive cells suggesting cellular apoptosis, and this was associated with RGC cell death.[44,45] Retinal sections were subjected to TUNEL staining following exposure to 2 months of elevated IOP. TUNEL-positive cells were observed in the inner retina of high IOP and high IOP + scrambled-transduced eyes. Shp2 KD under experimental glaucoma conditions markedly reduced the TUNEL apoptotic staining, which supported our histological data obtained from retina and optic nerve from Shp2-KD-subjected animals (Figures 7L and 7M). Proteomics analysis also supported these observations and indicated that proteins associated with cell death and apoptotic pathway were downregulated upon Shp2 silencing in glaucoma conditions (Nradd, Prdx3, Taok3, Set, and Mef2d) (Figure S9C).

Given that Shp2 upregulation in normal animals resulted in loss of inner retinal function, we investigated whether Shp2 silencing in glaucoma conditions could provide protection against the inner retinal functional deficits associated with the experimental glaucoma model. pSTR data indicated a significant decline in the amplitudes in animals that were exposed to chronically elevated IOP for 2 months (Figures 7N and 7O). Consistent with previous results, AAV2-Scrambled sequence transduction in high-IOP rats also resulted in a similar decline in the IOP amplitudes (n = 8) (Figures 7P and 7Q). A significant rescue of the pSTR amplitudes was observed in high-IOP animal groups that were subjected to AAV2-mediated Shp2 silencing (Figures 7N–7Q). No significant changes in whole retinal scotopic ERG response were observed in any of the experimental groups (n = 8 each) following IOP elevation or AAV2 transduction (Figures 7R–7U), indicating that the high IOP or protective effects of Shp2 suppression under elevated IOP conditions were mainly localized to the inner retina. Sustained Shp2 KD in adult retinas also did not have any noticeable effect on the PAX6 (amacrine cell), glial fibrillary acidic protein (GFAP; Müller cell), and CHX10 (bipolar cell) expression or localization in the retina as demonstrated by immunofluorescence staining (Figure S15). These data, along with previous results, demonstrated that while Shp2 overexpression has a detrimental inner retinal structural and functional phenotype in the adult animals, Shp2 silencing could rescue the experimental glaucoma deficits by rescuing both structural and functional losses.

DISCUSSION

This study established for the first time a previously unrecognized role of *Shp2* as a critical regulator of RGC survival in an experimental model of glaucoma with elevated IOP. The enzyme has been implicated in BDNF-dependent phosphorylation of TrkB and its activation,[17] and it interacts with TrkB in the isolated rat RGCs via the adaptor protein caveolin.[7] Mitogenic phosphatase Shp2 plays an important role during development and differentiation of RGCs, as evidenced in retinal degenerative changes including optic nerve dystrophy in $Shp2^{flox/flox}$ mutant mice.[46,47] Shp2 is also implicated in supporting the survival of the photoreceptors indirectly through its effects on the Müller cells.[46,48]

Our group and others have previously demonstrated that Shp2 interacts with TrkB in RGCs and other neuronal cells.[7,17] In this study, we discovered that modulation of Shp2 expression using AAV2 negatively regulated TrkB activity in the RGCs *in vivo*. Shp2 silencing, indeed, protected against inner retinal laminar structural and functional deficits induced by experimental glaucoma. Consistent with this, Shp2 upregulation induced increased ER stress, as well as loss of GCL density and inner retinal dysfunction in healthy animals.

There is growing evidence suggesting the critical role of neurotrophic factors, particularly with BDNF/TrkB and its downstream signaling, to support RGC survival, in studies using various models of optic

nerve injury. We previously reported that diminished BDNF/TrkB signaling pathways are associated with age related inner retinal degenerative phenotypes and that the exacerbation of experimental glaucoma induced RGC deficits.[37] In the current study, we modulated the expression of *Shp2* in healthy animal retina and also under elevated IOP conditions using an intravitreal injection of AAV2, employed within the CAG2 hybrid promoter. Our results show that sustained *Shp2* silencing suppressed apoptosis in the inner retinal layers under increased IOP and conversely that Shp2 upregulation in the RGCs promoted apoptosis in healthy retinas.

Intravitreal injection of AAV2 expressing Shp2 or Shp2-shRNA under the CAG2 hybrid promoter was effective in modulating the phosphatase expression in the GCL. We observed a sustained modulation of Shp2 for over 2 months in the retina, utilizing EGFP as a marker. We have previously shown that Shp2 interacts with TrkB in the isolated RGCs using co-immunoprecipitations[7] and also recently reported Shp2-TrkB interactions in the SH-SY5Y cells.[29] We and others have demonstrated that BDNF/TrkB signaling is critical for the RGC survival[37] and that BDNF administration is able to provide a transient protection to the RGCs under various experimental stress conditions.[49–51] For example, in a rat model of laser-induced experimental glaucoma, RGC loss was significantly reduced by AAV-transduced BDNF at 4 weeks post-laser-exposure to the trabecular meshwork.[52] Ren and colleagues[5] demonstrated that the visual evoked potential parameters were protected by BDNF for 9 weeks following a transient IOP spike; moreover, visual acuity and contrast sensitivity were well maintained for up to 1 year. The inability of exogenous BDNF administration to provide a sustained protection to RGCs[53] is attributed to simultaneous dephosphorylation induced by partner phosphatase Shp2.[7] Here, we specifically targeted Shp2 using AAV in the RGCs and determined its effects on the TrkB signaling.

To our knowledge, the effects of Shp2 modulation on TrkB under *in vivo* conditions have not been delineated previously, and this study provides first evidence that Shp2 inversely regulates TrkB activity in the inner retina, under both healthy and experimental glaucoma conditions. Given that there was no observable localization or expression changes in BDNF and total TrkB protein levels, pTrkB changes within RGCs are attributed to changes in tyrosine phosphatase activity of Shp2. Shp2 upregulation suppressed Erk1/2 activation, while its KD under both healthy and experimental glaucoma conditions led to significant Akt and Erk1/2 activation and deactivated the GSK3β signaling in the ONH. ONH tissue is enriched in RGC axons without the cell bodies, although it also contains a significant astrocyte cell population. This negative modulation of PI3K downstream signaling in the retinal tissue by Shp2 is a novel observation and is in contrast to the effects of Shp2 inhibition reported previously in $CD34^+$ cells and other tumor tissues.[54,55] Shp2 was shown to negatively affect PI3K/Akt activation induced by epidermal growth factor through its dephosphorylating effects on Gab1 adaptor protein.[56,57] On the other hand, TrkB activation promoted Akt and Erk signaling and exhibited an inhibitory effect on the GSK3β activation in the retinal neurons.[36,58,59] The PI3K signaling cascade has been consistently reported to be negatively regulated in the retinal tissues in both experimental glaucoma and human glaucoma.[37,60,61] In this study, we corroborated the previous findings of reduced PI3K downstream signaling in human glaucoma tissues and demonstrated that reduced pTrkB Y^{515} was associated with increased Shp2 expression levels in glaucoma. Similar Shp2 upregulation was also evident in the rat retinas that were exposed to chronically elevated IOP and was associated with reduced PI3K downstream signaling. Silencing Shp2 in the rat RGCs exposed to high IOP resurrected pTrkB and its downstream effectors pAkt and Erk1/2, with inhibitory effects on GSK3β. GSK3β activation has been shown to mediate apoptosis and cell death in cancer cells through its effects on the centrosome,[62] and it has also been implicated in neuronal apoptosis during early diabetic retinopathy.[63] Shp2 KD consistently resulted in increased phosphorylation of the TrkB downstream signaling molecules compared to scrambled controls, supporting our conclusion that Shp2 silencing in a glaucoma model resulted in activation of the TrkB downstream signaling (pAktS473, $^*p < 0.04$, n = 4; pErk T^{202}/Y^{204}, $^*p < 0.01$, n = 4; and pGsk3βS9, $^{**}p < 0.04$, n = 4). These findings were also supported by our results of Shp2 silencing effects on TrkB signaling in the retina under normal IOP conditions. Significantly increased pAktS473, pErk T^{202}/Y^{204}, and pGsk3βS9 phosphorylation were also observed in this experiment upon Shp2 KD.

Accordingly, we identified increased TUNEL staining in both Shp2-overexpressed retinas and in retinas subjected to chronically elevated IOP. Apoptotic staining was mitigated in the high-IOP retinas that were subjected to Shp2 suppression. Proteomic analysis also revealed the downregulation of apoptotic-pathway-associated proteins in the retinas subjected to Shp2 KD. Shp2 mutant mouse retinas have previously been reported to exhibit abnormal cell death in the GCL around P10,[46] and we also observed apoptotic staining predominantly localized to the inner retinal layers.

Shp2 has been shown to induce ER stress activation in hepatocytes and promote Ca^{2+} efflux from the ER.[64,65] ER stress is implicated in molecular pathologies associated with RGC degeneration; thus, modulating ER stress was suggested as a potential therapeutic strategy to rescue RGCs.[41,66,67] Additionally, upregulation of ER stress markers has been suggested to promote apoptotic changes in several studies.[68,69] We observed increased Bip, CHOP, XBP-1, and p-PERK levels in SH-SY5Y cells that were subjected to Shp2 upregulation.[29] In the course of this study, we established that Shp2 overexpression in RGCs resulted in an enhanced ER stress marker response, while its silencing in high-IOP conditions resulted in significant suppression of ER stress markers CHOP and p-PERK. ER stress activation was also observed in the human retinal tissues, suggesting that ER stress is an important factor in glaucoma pathogenesis that could potentially be modulated by inhibiting Shp2 in the RGCs.

The exact impact of the Shp2 modulation and its consequences on TrkB signaling and ER stress response were correlated with retinal structural and functional alterations. A prominent loss of the GCL density and reduced thickness of the IPL was observed in the retinas

that were subjected to Shp2 upregulation. IPL thinning may be attributed to reduced RGC dendrites that form a network of fibrils in this layer. Corroborating these findings, a reduced optic nerve axonal density further established degenerative changes in RGCs subjected to sustained Shp2 upregulation. pSTR amplitudes were reduced in Shp2-overexpressing retinas that further strengthened the hypothesis that sustained Shp2 upregulation in the RGCs had a detrimental impact on the inner retina. The most intriguing outcome was that Shp2 silencing in the experimental glaucoma animals provided protection against GCL thinning and optic nerve axonal loss. Deficits in retinal laminar structure such as reduced retinal thickness, rosette formation, and degenerated inner limiting membrane and nerve fiber layer have been previously reported in retinas that were subjected to Six3-Cre conditional ablation of Shp2.[46] Supporting our findings, severe atrophy and vacuolization of the optic nerve suggesting the loss of nerve fibers was also observed in these Shp2 mutant animals.[46] Remarkably, AAV2-mediated Shp2 silencing restored the inner retinal function as demonstrated by improved pSTR amplitudes. The role of Shp2 in regulating retinal function was evident from the previous study where Six3-Cre mediated conditional Shp2-ablated animals manifested wide-ranging deficits in rod and cone responses.[46] Similar loss of pSTR amplitudes was also observed in BDNF heterozygous mice with both increasing age and upon exposure to chronically elevated IOP.[37]

Shp2 deletion has previously been shown to induce apoptosis in retinal cells and has led to retinal structural and functional deficits;[46] however, these animals had been Shp2 genetically ablated from birth within the retina, which could potentially alter the post-natal retinal developmental trajectory. Shp2 has indeed been shown to be involved in regulating neuronal differentiation in early retinal development and control optic vesicle pattern through its effects on the retinal progenitor factors and cell proliferation.[19] In contrast, our study utilized adult animals and modulated Shp2 using AAV therapy, thus excluding development-related Shp2 roles within the retina. Further, our study used the RGC-specific promoter to modulate Shp2 expression, while the previous study involved the use Six3-Cre in Shp2-floxed animals, which shows widespread recombination in all the retinal layers.[46]

Overall, our results demonstrate a long-term functional, structural, and molecular inner retinal protection conferred by Shp2 KD in the eyes that were exposed to experimental glaucoma. This was in sharp contrast to the GFP-transduced control animals and highlighted that Shp2 targeting has the potential to provide a significant therapeutic benefit in glaucoma. Several biochemical aspects, however, such as Shp2 involvement in inducing ER stress response in the retina, requires further mechanistic insight. To our knowledge, this type of inner retinal functional and structural protection in glaucoma has not been linked to Shp2 regulation previously, despite well-established roles of BDNF/TrkB signaling in protecting the RGCs. A high degree of protection observed here can be attributed to the use of specific ganglion cell-hybrid promoters, appropriate AAV serotype, and efficient intravitreal delivery techniques, which supports the application of gene technology both as a means to understand the disease mechanisms as well as enhance neuroprotective pathways in glaucoma.

MATERIALS AND METHODS

Animals

Male Sprague-Dawley (SD) rats with a body weight of 300 to 350 g (10–12 weeks; Animal Research Centre, Perth, Australia) were used. All animals were maintained in an air-conditioned room with controlled temperature (21°C ± 2°C) and fixed daily 12-hr light/dark cycles. All procedures involving animals were conducted in accordance with the Australian Code of Practice for the Care and Use of Animals for Scientific Purposes and the guidelines of the ARVO statement for the use of animals in ophthalmic and vision Research and were approved by the Macquarie University Animal Ethics Committee in Australia. The animals were anaesthetized with an intraperitoneal (i.p.) injection of ketamine (75 mg/kg) and medetomidine (0.5 mg/kg) for all the procedures, including the intraocular microbead injections and retinal electrophysiological recordings.

Human Retinal Tissues

Human post-mortem retinal tissues from glaucoma and control subjects were obtained from the Sydney Eye Bank, Australia. Research was performed as per the principles outlined in the Declaration of Helsinki, and ethics approval was obtained from the Macquarie University Human Research Ethics Committee (5201200899). Ages of the eye donors ranged from 67 to 82 years (n = 4 each group). Eye tissues were collected within 6 hr after death. A history of glaucoma was obtained from the donor's medical records, and eyes with any other retinal pathology were excluded from the study. Using surgical microscope, human retinas was carefully harvested from the donor eye and ONH was removed from the isolated retinas. ONH lysates were used for immunoblotting. Small parts of retina with sclera were cut and then embedded in tissue Tek OCT cryostat embedding medium as described previously[70] for immunofluorescence.

Microbead Administration-Experimental Glaucoma Model

For microbead injection, animals were placed on a heating pad during the procedure, and both pupils were dilated with topical tropicamide 1% and anesthetized with alcaine 0.5% drops. Polystyrene microspheres (10 μm) were injected with a concentration of 1.0×10^6 beads/mL (vol 10 μL) (FluoSpheres; Invitrogen, USA) followed by an air bubble using a Hamilton syringe connected to disposable 33G needle (TSK Laboratory, Tochigi, Japan). All procedures were performed using an operating microscope (OPMI-11; Carl Zeiss, Germany) with care taken to avoid needle contact with the iris or lens. One of the eyes was randomly selected for injection, leaving the fellow eye as control. Microbead injection was performed weekly between week 0 and week 4 and then fortnightly till week 8. The IOP was monitored in rats using an iCare TonoLab (Tonovet; Icare, Finland) as described previously.[37]

AAV Construct Design

The murine Shp2 cDNA (BC057398, isoform-a) was placed under the transcriptional control of the cytomegalovirus (CMV) chicken

β-actin rabbit beta-globin gene (CAG2) hybrid promoter and inserted into the AAV2 EGFP vector (AAV2-CAG2-EGFP-T2A-mShp2 or AAV2-Shp2) for Shp2 overexpression (Vector Biolabs, USA). For *Shp2* gene silencing, shRNAmir was used to knock down the Shp2 sequence (AAV2-CAG-EGFP-mShp2-shRNAmir or AAV2-Shp2KD). AAV2 containing shRNAs targeting Shp2 coding sequences (NM_001109992.1) starting at nucleotide 1296 (5′-CCTGATGAGTATGCGCTCAAA-3′) was used to achieve Shp2 KD with 5′-GTCTCCACGCGCAGTACATTT-3′ sequence as scrambled shRNAmir control as described previously.[29]

AAV2 Vector Intravitreal Administration

Animals were anesthetized and pupils dilated with 1% tropicamide as described previously.[37] AAV solution was administered using a 33G needle (5 μL) injected temporally and nasally at a 45° angle 2 mm behind the corneoscleral limbus into the vitreous avoiding lens. All injections were carefully performed under operating surgical microscope (OPMI-11; Carl Zeiss, Germany). After injection, the needle was left in place for another minute to allow dispersion of the AAV solution into the vitreous. Control eyes were injected with AAV encoding scrambled sequence or with vehicle treatment. The animals were monitored for 2 months after the AAV2 administration. IOP of all eyes was monitored using lab tonometer (Icare-LAB, USA) and four consecutive IOP readings were obtained from each eye.

Electroretinography

Electroretinographic (ERG) recordings were performed as described previously.[71] The rats were dark-adapted overnight and anaesthetised with ketamine and medetomidine (75 and 0.5 mg/kg, respectively), and pupils were dilated using 1% tropicamide and topical anesthetic (1% alcaine) applied to the cornea. Ground and reference electrodes were placed subcutaneously in the tail and forehead of the animal, respectively. A solid custom-made gold ring recording electrode (Roland Consult, Germany) was placed on each eye in contact with the cornea, and methylcellulose applied to maintain contact between the cornea and the electrode. ERGs were recorded using a flash intensity of 3 log cd·s/m^2 (Ocusciences, USA). For all ERG recordings, a-wave amplitude was measured from baseline to the a-wave trough; b-wave was measured from the a-wave trough to the peak of b-wave. For pSTRs, dim stimulation using flash intensities of −4 log cd·s/m^2 (0.5 Hz) was delivered 30 times. pSTR amplitudes were measured from baseline to the positive peak observed around 120 ms.

Retinal Section Histology and GCL Counting

Animals were euthanized with an overdose of pentobarbitone followed by transcardial perfusion using 4% paraformaldehyde. Eyes were marked for orientation, harvested, and fixed in 4% paraformaldehyde. 5- to 7-μm-thick sagittal sections of the eye[61] were obtained and subjected to H&E staining as described previously.[37,61] GCL density was determined by counting the number of cells (100–600 μm from the edge of the optic disc) using light microscopy (Carl Zeiss). Inner nuclear and inner plexiform layer thickness was evaluated and compared between *SHP2* upregulation and downregulated retinas. For GCL density, six sections from each eye were analyzed for quantification. For retinal thickness changes, 15 sections per eye were stained for each group (n = 4 per group).

Optic Nerve Section Histology and Axon Counting

Optic nerve was similarly treated as for whole eye/retina and 2- to 5-μm-thick cross-sections were subjected to PPD[72] and Bielschowsky's silver staining as reported previously.[61] Light microscopic images were captured at low and high magnification using Zeiss microscope (Axio Imager microscope, Zeiss). The number of axons counted (10^{-2} mm^2) manually across the entire cross-section photographed at high magnification. Degenerative profiles was performed in PPD-stained optic nerve cross-section by counting number of axons with swelling and were calculated as ratio of degenerative profiles in healthy and treated eyes.[73] Changes in axonal density was evaluated in optic nerve silver stain cross-section. Six images for each optic nerve were analyzed to compute axon counts per group (n = 3 optic nerves per group).[70]

SDS-PAGE and Western Blotting

Eyes were enucleated and ONH regions of the retina surgically excised from the retina under a microscope and lysed (20 mM HEPES [pH 7.4], 1% Triton X-100, 1 mM EDTA) containing PhosSTOP (Sigma) and protease inhibitor cocktail (Sigma). Protein concentrations were assessed using the bicinchoninic acid (BCA) protein estimation.[74] Proteins were resolved using 10% SDS-PAGE and transferred to polyvinylidene fluoride (PVDF) membranes (Invitrogen). Membranes were blocked in Tris-buffered saline (TTBS) (20 mM Tris-HCl [pH 7.4], 100 mM NaCl, and 0.1% Tween 20) containing 5% skimmed milk[75,76] and incubated overnight with either of the antibodies as indicated-anti-GFP (1:1,000), anti-p-Shp2(Y^{542}) (1:1,000), anti-Shp2 (1:1,000), anti-p-TrkB Y^{515} (1:1,000), anti-TrkB (1:1,000), anti-p-Akt(S^{473}) (1:1,000), anti-Akt (1:1,000), anti-p-Erk(T^{202}/Y^{204}) (1:1,000), anti-pGsk3β(S^{9}) (1:1,000), anti-Gsk3β (1:1,000), anti-Grp78 (1:400), anti-CHOP (1:400), anti-p-PERK (1:400), and anti-actin (1:5,000) overnight at 4°C (Table S1). Following primary antibody treatment, blots were incubated with horseradish peroxidase (HRP)-linked secondary antibodies and signal detected using supersignal west pico chemiluminescent substrate (Pierce). Signals were detected using an automated luminescent image analyzer (ImageQuant LAS 4000). Densitometric quantification of the band intensities was evaluated using ImageJ software (NIH, USA).[59]

Tandem Mass Tags Labeling and Proteomic Analysis of Retinal Samples

Proteins extracts were suspended in 2% SDS in 50 mM Tris-HCl (pH 8.8). The samples were digested in solution using trypsin at 37°C. Tandem mass tag (TMT) labeling of the resulting peptides was achieved with respective reporter ions at m/z = 126, 127N, 127C, 128N, 128C, 129N, 129C, 130N, 130C, and 131 as reported previously.[39] The samples were pooled, desalted by solid-phase extraction, and fractionated using cation exchange HPLC. Desalting was carried out using C18 OMIXtips (Agilent) and samples analyzed using Q Exactive Orbitrap mass spectrometer coupled to an EASY-nLC1000 (Thermo Scientific). Data generated was processed using

Proteome Discoverer v1.4 (Thermo Scientific) and MASCOT server (v 2.3; Matrix Science, UK). The tandem mass spectrometry (MS/MS) spectra were subjected to blast against NCBI *Rattus norvegicus* protein database. The output files were further processed using the TMTPrepPro scripts accessed through a graphical user interface.[77]

Immunofluorescence Analysis

The enucleated animal eyes were fixed for 2 hr in 4% freshly prepared paraformaldehyde (PFA). The eyes were washed with 1× PBS to remove PFA and incubated in 30% sucrose overnight for cryoprotection. The eyes were then embedded in tissue Tek optimum cutting temperature (OCT) cryostat embedding medium as described previously,[70] flash frozen in liquid N_2 and stored at −80°C. Tissue sections 12-μm thick were prepared using a cryostat (Leica). Before immunostaining, slides were warmed at 37°C for 30 min and washed twice with 1× PBS for 10 min. Using pep-pen, the tissue area was circled and incubated in blocking buffer solution with 5% goat serum and sections permeabilized with 0.3% Triton X-100 in 1× PBS[61] for 60 min. The blocking buffer solution was aspirated, sections incubated with the indicated primary antibodies overnight at 4°C prepared in antibody dilution buffer (1× PBS/1% BSA/0.3% Triton X-100). The following antibodies were used for immunohistochemistry: anti-Shp2 (1:250), anti-p-Shp2 (Y^{542}) (1:250), anti-GFP (1:500), anti-p-TrkB Y^{515} (1:200), anti-TrkB (1:200), anti-CHOP (1:250), anti-p-PERK (1:250), anti-BDNF (1:250), anti-Pax6 (1:400), anti-GFAP (1:400), anti-Chx10 (1:400), anti-NeuN (1:1,000) and βIII-tubulin (1:500) (Table S1). The slides were then rinsed three times in 1× PBS for 5 min each and incubated with either of the secondary Cy3, Alexa Fluor 488, Alexa Fluor 647, or fluorescein isothiocyanate (FITC)-conjugated anti-rabbit (1:400), anti-mouse (1:400), or anti-goat (1:200) for 1–2 hr at room temperature in the dark followed by washing three times in 1× PBS for 5 min each and mounted using anti-fade mounting media with Prolong DAPI and was allowed to dry at room temperature. Images were acquired using a Zeiss fluorescence microscope (Axio Imager microscope Zeiss).[78] GFP^+/total cells and $Shp2^+$/total cells in Figures 1E and 1F were quantified manually using 10 sections from each animal eye (n = 4).

TUNEL-Apoptosis Assay

Cell apoptosis in animal retinas was detected using a TUNEL from Promega, DeadEnd Fluorometric TUNEL System as described previously.[29] PFA-fixed frozen cryostat sections were warmed at 37°C for 30 min and washed two times with 1× PBS for 5 min each. The sections were then permeabilized by adding 100 μL of a 20 μg/mL Proteinase K solution and were allowed to incubate at room temperature for 10–15 min. It was washed twice in 1× PBS and was re-fixed in 4% PFA for 5 min. Before addition of 100 μL equilibration buffer, the slides were washed in 1× PBS for 5 min. Labeling was performed by adding 50 μL of TdT reaction mix to the tissue. To prevent tissue from getting dry and for even distribution of mix, a plastic coverslip was placed over the slides, and slides were incubated for 60 min at 37°C in a humidified chamber in the dark. Following incubation, reaction was stopped by immersing the slides (without plastic coverslips) in 2× saline-sodium citrate (SSC) buffer for 15 min. Slides were washed with 1× PBS, mounted with prolong antifade DAPI, and directly analyzed for apoptotic cell staining using epi-fluorescence microscopy.

Statistical Analysis

The changes in ERG/STR amplitudes, retinal thickness, optic nerve axonal density, western blot, histology, and TUNEL data were analyzed using GraphPad Prism (v 6.0) (GraphPad Software, San Diego, CA). All data are represented as the mean ± SD. Statistical analysis was performed using Student's t test for unpaired groups or one-way ANOVA followed with Bonferroni's post-hoc multiple comparisons test. All values with error bars are presented as mean ± SD for given n sizes. The significance value was set at $p < 0.05$. All error bars indicate SD in the figure legends.

SUPPLEMENTAL INFORMATION

Supplemental Information includes fifteen figures, one table, and one data file and can be found with this article online at https://doi.org/10.1016/j.ymthe.2018.09.019.

AUTHOR CONTRIBUTIONS

N.C. conceived, designed, performed, analyzed animal experiments and interpreted the data, prepared figures, and wrote the manuscript. Y.D. performed the experiments. M.M. conducted the proteomics experiment and interpreted the data. Y.W. conducted the proteomics experiment and interpreted the data. G.H.S. conducted the proteomics experiment. M.A. and R.V.W. performed animal experiments and helped in animal monitoring. Veer Gupta and Y.Y. critically revised the manuscript. S.L.G. developed the concept, wrote the manuscript, and led and supervised the studies. Vivek Gupta conceived, designed, analyzed and interpreted the data, participated in writing and critically revising the manuscript, and supervised the studies.

CONFLICTS OF INTEREST

The authors have no conflicts of interest.

ACKNOWLEDGMENTS

We acknowledge the support from Ophthalmic Research Institute of Australia (ORIA, 9201400700), the Hillcrest Foundation (2018/0677), Macquarie University (5016420), and the National Health and Medical Research Council (NHMRC, 1084767 and 1139560).

REFERENCES

1. Katz, B., Weinreb, R.N., Wheeler, D.T., and Klauber, M.R. (1990). Anterior ischaemic optic neuropathy and intraocular pressure. Br. J. Ophthalmol. *74*, 99–102.

2. Gossman, C.A., Christie, J., Webster, M.K., Linn, D.M., and Linn, C.L. (2016). Neuroprotective Strategies in Glaucoma. Curr. Pharm. Des. *22*, 2178–2192.

3. Foldvari, M., and Chen, D.W. (2016). The intricacies of neurotrophic factor therapy for retinal ganglion cell rescue in glaucoma: a case for gene therapy. Neural Regen. Res. *11*, 875–877.

4. Galindo-Romero, C., Valiente-Soriano, F.J., Jiménez-López, M., García-Ayuso, D., Villegas-Pérez, M.P., Vidal-Sanz, M., and Agudo-Barriuso, M. (2013). Effect of brain-derived neurotrophic factor on mouse axotomized retinal ganglion cells and phagocytic microglia. Invest. Ophthalmol. Vis. Sci. *54*, 974–985.

5. Ren, R., Li, Y., Liu, Z., Liu, K., and He, S. (2012). Long-term rescue of rat retinal ganglion cells and visual function by AAV-mediated BDNF expression after acute elevation of intraocular pressure. Invest. Ophthalmol. Vis. Sci. *53*, 1003–1011.

6. Cheng, L., Sapieha, P., Kittlerova, P., Hauswirth, W.W., and Di Polo, A. (2002). TrkB gene transfer protects retinal ganglion cells from axotomy-induced death in vivo. J. Neurosci. *22*, 3977–3986.

7. Gupta, V.K., You, Y., Klistorner, A., and Graham, S.L. (2012). Shp-2 regulates the TrkB receptor activity in the retinal ganglion cells under glaucomatous stress. Biochim. Biophys. Acta *1822*, 1643–1649.

8. Numakawa, T., Suzuki, S., Kumamaru, E., Adachi, N., Richards, M., and Kunugi, H. (2010). BDNF function and intracellular signaling in neurons. Histol. Histopathol. *25*, 237–258.

9. Hua, Z., Gu, X., Dong, Y., Tan, F., Liu, Z., Thiele, C.J., and Li, Z. (2016). PI3K and MAPK pathways mediate the BDNF/TrkB-increased metastasis in neuroblastoma. Tumour Biol. *37*, 16227–16236.

10. Chitranshi, N., Dheer, Y., Abbasi, M., You, Y., Graham, S.L., and Gupta, V. (2018). Glaucoma Pathogenesis and Neurotrophins: Focus on the Molecular and Genetic Basis for Therapeutic Prospects. Curr. Neuropharmacol. *16*, 1018–1035.

11. Igarashi, T., Miyake, K., Kobayashi, M., Kameya, S., Fujimoto, C., Nakamoto, K., Takahashi, H., Igarashi, T., Miyake, N., Iijima, O., et al. (2016). Tyrosine triple mutated AAV2-BDNF gene therapy in a rat model of transient IOP elevation. Mol. Vis. *22*, 816–826.

12. Domenici, L., Origlia, N., Falsini, B., Cerri, E., Barloscio, D., Fabiani, C., Sansò, M., and Giovannini, L. (2014). Rescue of retinal function by BDNF in a mouse model of glaucoma. PLoS ONE *9*, e115579.

13. Guillin, O., Diaz, J., Carroll, P., Griffon, N., Schwartz, J.C., and Sokoloff, P. (2001). BDNF controls dopamine D3 receptor expression and triggers behavioural sensitization. Nature *411*, 86–89.

14. Sandhya, V.K., Raju, R., Verma, R., Advani, J., Sharma, R., Radhakrishnan, A., Nanjappa, V., Narayana, J., Somani, B.L., Mukherjee, K.K., et al. (2013). A network map of BDNF/TRKB and BDNF/p75NTR signaling system. J. Cell Commun. Signal. *7*, 301–307.

15. Lin, S.Y., Wu, K., Levine, E.S., Mount, H.T., Suen, P.C., and Black, I.B. (1998). BDNF acutely increases tyrosine phosphorylation of the NMDA receptor subunit 2B in cortical and hippocampal postsynaptic densities. Brain Res. Mol. Brain Res. *55*, 20–27.

16. Kumamaru, E., Numakawa, T., Adachi, N., and Kunugi, H. (2011). Glucocorticoid suppresses BDNF-stimulated MAPK/ERK pathway via inhibiting interaction of Shp2 with TrkB. FEBS Lett. *585*, 3224–3228.

17. Rusanescu, G., Yang, W., Bai, A., Neel, B.G., and Feig, L.A. (2005). Tyrosine phosphatase SHP-2 is a mediator of activity-dependent neuronal excitotoxicity. EMBO J. *24*, 305–314.

18. Suzuki, T., Matozaki, T., Mizoguchi, A., and Kasuga, M. (1995). Localization and subcellular distribution of SH-PTP2, a protein-tyrosine phosphatase with Src homology-2 domains, in rat brain. Biochem. Biophys. Res. Commun. *211*, 950–959.

19. Cai, Z., Feng, G.S., and Zhang, X. (2010). Temporal requirement of the protein tyrosine phosphatase Shp2 in establishing the neuronal fate in early retinal development. J. Neurosci. *30*, 4110–4119.

20. Ralston, A., and Rossant, J. (2006). How signaling promotes stem cell survival: trophoblast stem cells and Shp2. Dev. Cell *10*, 275–276.

21. Chong, Z.Z., Lin, S.H., Kang, J.Q., and Maiese, K. (2003). The tyrosine phosphatase SHP2 modulates MAP kinase p38 and caspase 1 and 3 to foster neuronal survival. Cell. Mol. Neurobiol. *23*, 561–578.

22. Goldsmith, B.A., and Koizumi, S. (1997). Transient association of the phosphotyrosine phosphatase SHP-2 with TrkA is induced by nerve growth factor. J. Neurochem. *69*, 1014–1019.

23. Zhang, S.S., Hao, E., Yu, J., Liu, W., Wang, J., Levine, F., and Feng, G.S. (2009). Coordinated regulation by Shp2 tyrosine phosphatase of signaling events controlling insulin biosynthesis in pancreatic beta-cells. Proc. Natl. Acad. Sci. USA *106*, 7531–7536.

24. Ahrendsen, J.T., Harlow, D.E., Finseth, L.T., Bourne, J.N., Hickey, S.P., Gould, E.A., Culp, C.M., and Macklin, W.B. (2018). The Protein Tyrosine Phosphatase Shp2 Regulates Oligodendrocyte Differentiation and Early Myelination and Contributes to Timely Remyelination. J. Neurosci. *38*, 787–802.

25. Grossmann, K.S., Wende, H., Paul, F.E., Cheret, C., Garratt, A.N., Zurborg, S., Feinberg, K., Besser, D., Schulz, H., Peles, E., et al. (2009). The tyrosine phosphatase Shp2 (PTPN11) directs Neuregulin-1/ErbB signaling throughout Schwann cell development. Proc. Natl. Acad. Sci. USA *106*, 16704–16709.

26. Kang, H.J., Chung, D.H., Sung, C.O., Yoo, S.H., Yu, E., Kim, N., Lee, S.H., Song, J.Y., Kim, C.J., and Choi, J. (2017). SHP2 is induced by the HBx-NF-κB pathway and contributes to fibrosis during human early hepatocellular carcinoma development. Oncotarget *8*, 27263–27276.

27. Ke, Y., Zhang, E.E., Hagihara, K., Wu, D., Pang, Y., Klein, R., Curran, T., Ranscht, B., and Feng, G.S. (2007). Deletion of Shp2 in the brain leads to defective proliferation and differentiation in neural stem cells and early postnatal lethality. Mol. Cell. Biol. *27*, 6706–6717.

28. Aoki, Y., Huang, Z., Thomas, S.S., Bhide, P.G., Huang, I., Moskowitz, M.A., and Reeves, S.A. (2000). Increased susceptibility to ischemia-induced brain damage in transgenic mice overexpressing a dominant negative form of SHP2. FASEB J. *14*, 1965–1973.

29. Chitranshi, N., Dheer, Y., Gupta, V., Abbasi, M., Mirzaei, M., You, Y., Chung, R., Graham, S.L., and Gupta, V. (2017). PTPN11 induces endoplasmic stress and apoptosis in SH-SY5Y cells. Neuroscience *364*, 175–189.

30. Smith, C.A., and Chauhan, B.C. (2018). In vivo imaging of adeno-associated viral vector labelled retinal ganglion cells. Sci. Rep. *8*, 1490.

31. Hanlon, K.S., Chadderton, N., Palfi, A., Blanco Fernandez, A., Humphries, P., Kenna, P.F., Millington-Ward, S., and Farrar, G.J. (2017). A Novel Retinal Ganglion Cell Promoter for Utility in AAV Vectors. Front. Neurosci. *11*, 521.

32. Huang, Z., Hu, Z., Xie, P., and Liu, Q. (2017). Tyrosine-mutated AAV2-mediated shRNA silencing of PTEN promotes axon regeneration of adult optic nerve. PLoS ONE *12*, e0174096.

33. Mysona, B.A., Zhao, J., and Bollinger, K.E. (2017). Role of BDNF/TrkB pathway in the visual system: Therapeutic implications for glaucoma. Expert Rev. Ophthalmol. *12*, 69–81.

34. Yang, W., Klaman, L.D., Chen, B., Araki, T., Harada, H., Thomas, S.M., George, E.L., and Neel, B.G. (2006). An Shp2/SFK/Ras/Erk signaling pathway controls trophoblast stem cell survival. Dev. Cell *10*, 317–327.

35. Park, H., and Poo, M.M. (2013). Neurotrophin regulation of neural circuit development and function. Nat. Rev. Neurosci. *14*, 7–23.

36. Liu, Y., Tao, L., Fu, X., Zhao, Y., and Xu, X. (2013). BDNF protects retinal neurons from hyperglycemia through the TrkB/ERK/MAPK pathway. Mol. Med. Rep. *7*, 1773–1778.

37. Gupta, V., You, Y., Li, J., Gupta, V., Golzan, M., Klistorner, A., van den Buuse, M., and Graham, S. (2014). BDNF impairment is associated with age-related changes in the inner retina and exacerbates experimental glaucoma. Biochim. Biophys. Acta *1842*, 1567–1578.

38. Piri, N., Kwong, J.M., and Caprioli, J. (2013). Crystallins in retinal ganglion cell survival and regeneration. Mol. Neurobiol. *48*, 819–828.

39. Mirzaei, M., Gupta, V.B., Chick, J.M., Greco, T.M., Wu, Y., Chitranshi, N., Wall, R.V., Hone, E., Deng, L., Dheer, Y., et al. (2017). Age-related neurodegenerative disease associated pathways identified in retinal and vitreous proteome from human glaucoma eyes. Sci. Rep. *7*, 12685.

40. Piri, N., Song, M., Kwong, J.M.K., and Caprioli, J. (2006). Expression of Crystallin Genes Is Downregulated in Experimental Glaucoma. Invest. Ophthalmol. Vis. Sci. *47*, 1825.

41. Yang, L., Li, S., Miao, L., Huang, H., Liang, F., Teng, X., Xu, L., Wang, Q., Xiao, W., Ridder, W.H., 3rd, et al. (2016). Rescue of Glaucomatous Neurodegeneration by Differentially Modulating Neuronal Endoplasmic Reticulum Stress Molecules. J. Neurosci. *36*, 5891–5903.

42. Wang, M., Wey, S., Zhang, Y., Ye, R., and Lee, A.S. (2009). Role of the unfolded protein response regulator GRP78/BiP in development, cancer, and neurological disorders. Antioxid. Redox Signal. *11*, 2307–2316.

43. Peters, J.C., Bhattacharya, S., Clark, A.F., and Zode, G.S. (2015). Increased Endoplasmic Reticulum Stress in Human Glaucomatous Trabecular Meshwork Cells and Tissues. Invest. Ophthalmol. Vis. Sci. *56*, 3860–3868.

44. Guo, L., Moss, S.E., Alexander, R.A., Ali, R.R., Fitzke, F.W., and Cordeiro, M.F. (2005). Retinal ganglion cell apoptosis in glaucoma is related to intraocular pressure and IOP-induced effects on extracellular matrix. Invest. Ophthalmol. Vis. Sci. *46*, 175–182.

45. Smedowski, A., Pietrucha-Dutczak, M., Kaarniranta, K., and Lewin-Kowalik, J. (2014). A rat experimental model of glaucoma incorporating rapid-onset elevation of intraocular pressure. Sci. Rep. *4*, 5910.

46. Cai, Z., Simons, D.L., Fu, X.Y., Feng, G.S., Wu, S.M., and Zhang, X. (2011). Loss of Shp2-mediated mitogen-activated protein kinase signaling in Muller glial cells results in retinal degeneration. Mol. Cell. Biol. *31*, 2973–2983.

47. Pinzon-Guzman, C., Xing, T., Zhang, S.S., and Barnstable, C.J. (2015). Regulation of rod photoreceptor differentiation by STAT3 is controlled by a tyrosine phosphatase. J. Mol. Neurosci. *55*, 152–159.

48. Kinkl, N., Hageman, G.S., Sahel, J.A., and Hicks, D. (2002). Fibroblast growth factor receptor (FGFR) and candidate signaling molecule distribution within rat and human retina. Mol. Vis. *8*, 149–160.

49. Chen, H., and Weber, A.J. (2001). BDNF enhances retinal ganglion cell survival in cats with optic nerve damage. Invest. Ophthalmol. Vis. Sci. *42*, 966–974.

50. Wilson, A.M., and Di Polo, A. (2012). Gene therapy for retinal ganglion cell neuroprotection in glaucoma. Gene Ther. *19*, 127–136.

51. Martin, K.R., Quigley, H.A., Zack, D.J., Levkovitch-Verbin, H., Kielczewski, J., Valenta, D., Baumrind, L., Pease, M.E., Klein, R.L., and Hauswirth, W.W. (2003). Gene therapy with brain-derived neurotrophic factor as a protection: retinal ganglion cells in a rat glaucoma model. Invest. Ophthalmol. Vis. Sci. *44*, 4357–4365.

52. Fu, C.T., and Sretavan, D. (2010). Laser-induced ocular hypertension in albino CD-1 mice. Invest. Ophthalmol. Vis. Sci. *51*, 980–990.

53. Mansour-Robaey, S., Clarke, D.B., Wang, Y.C., Bray, G.M., and Aguayo, A.J. (1994). Effects of ocular injury and administration of brain-derived neurotrophic factor on survival and regrowth of axotomized retinal ganglion cells. Proc. Natl. Acad. Sci. USA *91*, 1632–1636.

54. Bunda, S., Burrell, K., Heir, P., Zeng, L., Alamsahebpour, A., Kano, Y., Raught, B., Zhang, Z.Y., Zadeh, G., and Ohh, M. (2015). Inhibition of SHP2-mediated dephosphorylation of Ras suppresses oncogenesis. Nat. Commun. *6*, 8859.

55. Li, L., Modi, H., McDonald, T., Rossi, J., Yee, J.K., and Bhatia, R. (2011). A critical role for SHP2 in STAT5 activation and growth factor-mediated proliferation, survival, and differentiation of human CD34+ cells. Blood *118*, 1504–1515.

56. Zhang, S.Q., Tsiaras, W.G., Araki, T., Wen, G., Minichiello, L., Klein, R., and Neel, B.G. (2002). Receptor-specific regulation of phosphatidylinositol 3′-kinase activation by the protein tyrosine phosphatase Shp2. Mol. Cell. Biol. *22*, 4062–4072.

57. Mattoon, D.R., Lamothe, B., Lax, I., and Schlessinger, J. (2004). The docking protein Gab1 is the primary mediator of EGF-stimulated activation of the PI-3K/Akt cell survival pathway. BMC Biol. *2*, 24.

58. Hu, Y., Cho, S., and Goldberg, J.L. (2010). Neurotrophic effect of a novel TrkB agonist on retinal ganglion cells. Invest. Ophthalmol. Vis. Sci. *51*, 1747–1754.

59. Gupta, V., Chitranshi, N., You, Y., Gupta, V., Klistorner, A., and Graham, S. (2014). Brain derived neurotrophic factor is involved in the regulation of glycogen synthase kinase 3β (GSK3β) signalling. Biochem. Biophys. Res. Commun. *454*, 381–386.

60. Fujita, Y., Sato, A., and Yamashita, T. (2013). Brimonidine promotes axon growth after optic nerve injury through Erk phosphorylation. Cell Death Dis. *4*, e763.

61. You, Y., Gupta, V.K., Li, J.C., Al-Adawy, N., Klistorner, A., and Graham, S.L. (2014). FTY720 protects retinal ganglion cells in experimental glaucoma. Invest. Ophthalmol. Vis. Sci. *55*, 3060–3066.

62. Yoshino, Y., and Ishioka, C. (2015). Inhibition of glycogen synthase kinase-3 beta induces apoptosis and mitotic catastrophe by disrupting centrosome regulation in cancer cells. Sci. Rep. *5*, 13249.

63. Li, Z., Ma, L., Chen, X., Li, Y., Li, S., Zhang, J., and Lu, L. (2014). Glycogen synthase kinase-3: a key kinase in retinal neuron apoptosis in early diabetic retinopathy. Chin. Med. J. (Engl.) *127*, 3464–3470.

64. Nagata, N., Matsuo, K., Bettaieb, A., Bakke, J., Matsuo, I., Graham, J., Xi, Y., Liu, S., Tomilov, A., Tomilova, N., et al. (2012). Hepatic Src homology phosphatase 2 regulates energy balance in mice. Endocrinology *153*, 3158–3169.

65. Wang, Q., Herrera Abreu, M.T., Siminovitch, K., Downey, G.P., and McCulloch, C.A. (2006). Phosphorylation of SHP-2 regulates interactions between the endoplasmic reticulum and focal adhesions to restrict interleukin-1-induced Ca2+ signaling. J. Biol. Chem. *281*, 31093–31105.

66. Doh, S.H., Kim, J.H., Lee, K.M., Park, H.Y., and Park, C.K. (2010). Retinal ganglion cell death induced by endoplasmic reticulum stress in a chronic glaucoma model. Brain Res. *1308*, 158–166.

67. Shimazawa, M., Inokuchi, Y., Ito, Y., Murata, H., Aihara, M., Miura, M., Araie, M., and Hara, H. (2007). Involvement of ER stress in retinal cell death. Mol. Vis. *13*, 578–587.

68. Abhishek, A., Benita, S., Kumari, M., Ganesan, D., Paul, E., Sasikumar, P., Mahesh, A., Yuvaraj, S., Ramprasath, T., and Selvam, G.S. (2017). Molecular analysis of oxalate-induced endoplasmic reticulum stress mediated apoptosis in the pathogenesis of kidney stone disease. J. Physiol. Biochem. *73*, 561–573.

69. Yuan, J., Chen, M., Xu, Q., Liang, J., Chen, R., Xiao, Y., Fang, M., and Chen, L. (2017). Effect of the Diabetic Environment On the Expression of MiRNAs in Endothelial Cells: Mir-149-5p Restoration Ameliorates the High Glucose-Induced Expression of TNF-α and ER Stress Markers. Cell. Physiol. Biochem. *43*, 120–135.

70. Gupta, V.K., Chitranshi, N., Gupta, V.B., Golzan, M., Dheer, Y., Wall, R.V., Georgevsky, D., King, A.E., Vickers, J.C., Chung, R., and Graham, S. (2016). Amyloid β accumulation and inner retinal degenerative changes in Alzheimer's disease transgenic mouse. Neurosci. Lett. *623*, 52–56.

71. Richards, A., Emondi, A.A., and Rohrer, B. (2006). Long-term ERG analysis in the partially light-damaged mouse retina reveals regressive and compensatory changes. Vis. Neurosci. *23*, 91–97.

72. Zarei, K., Scheetz, T.E., Christopher, M., Miller, K., Hedberg-Buenz, A., Tandon, A., Anderson, M.G., Fingert, J.H., and Abràmoff, M.D. (2016). Automated Axon Counting in Rodent Optic Nerve Sections with AxonJ. Sci. Rep. *6*, 26559.

73. Joos, K.M., Li, C., and Sappington, R.M. (2010). Morphometric changes in the rat optic nerve following short-term intermittent elevations in intraocular pressure. Invest. Ophthalmol. Vis. Sci. *51*, 6431–6440.

74. Basavarajappa, D.K., Gupta, V.K., Dighe, R., Rajala, A., and Rajala, R.V. (2011). Phosphorylated Grb14 is an endogenous inhibitor of retinal protein tyrosine phosphatase 1B, and light-dependent activation of Src phosphorylates Grb14. Mol. Cell. Biol. *31*, 3975–3987.

75. Gupta, V.K., Rajala, A., and Rajala, R.V. (2012). Insulin receptor regulates photoreceptor CNG channel activity. Am. J. Physiol. Endocrinol. Metab. *303*, E1363–E1372.

76. Gupta, V.K., Rajala, A., Daly, R.J., and Rajala, R.V. (2010). Growth factor receptor-bound protein 14: a new modulator of photoreceptor-specific cyclic-nucleotide-gated channel. EMBO Rep. *11*, 861–867.

77. Mirzaei, M., Pascovici, D., Wu, J.X., Chick, J., Wu, Y., Cooke, B., Haynes, P., and Molloy, M.P. (2017). TMT One-Stop Shop: From Reliable Sample Preparation to Computational Analysis Platform. Methods Mol. Biol. *1549*, 45–66.

78. Rajala, A., Gupta, V.K., Anderson, R.E., and Rajala, R.V. (2013). Light activation of the insulin receptor regulates mitochondrial hexokinase. A possible mechanism of retinal neuroprotection. Mitochondrion *13*, 566–576.